Master's Thesis

High-chromaticity Optics for the MAX IV 3 GeV Storage Ring

by

Teresia Olsson

Supervisor: Simon C. Leemann

September, 2013

Department of Electrical and Information Technology
Faculty of Engineering, LTH, Lund University
SE-221 00 Lund, Sweden

Abstract

The MAX IV facility is a 3rd generation state-of-the-art synchrotron light source currently under construction in Lund, Sweden. The MAX IV 3 GeV storage ring has a large negative natural chromaticity, which has to be corrected to positive values to prevent head-tail instabilities. On the other hand, high linear chromaticity can lead to a large tune footprint limiting Touschek lifetime. Therefore, the linear chromaticity is corrected to +1 in both planes with sextupoles while both sextupoles and octupoles are used to optimise the tune footprint. Studies indicate this design leads to threshold currents for resistive wall and transverse mode coupling instabilities beyond what is expected during regular user operation. However, since these are preliminary studies based on several approximations, the possibility of instability issues during commissioning needs to be considered. A short term solution is to operate the storage ring at a higher chromaticity. This thesis describes the development of a high-chromaticity optics for the MAX IV 3 GeV storage ring with linear chromaticity +4 in both planes. It focuses on reduction of chromatic and amplitude-dependent tune shifts to maximize dynamic aperture and Touschek lifetime. A comparison between the performance of the high-chromaticity optics and the design optics is also presented. The analysis reveals that the performance of the developed high-chromaticity optics is, not quite unexpectedly, poorer than the performance of the design optics. However, the performance of the high-chromaticity optics is estimated to be sufficient to allow the optics to be applied in the MAX IV 3 GeV storage ring as a short term solution if instability issues should occur during commissioning.

Acknowledgements

I wish to thank Martin Johansson for creating 2D simulations of the MAX IV 3 GeV sextupole and octupole magnets, for doing the simulations of the octupole magnets and for explaining to me how to do the same for the sextupole magnets. It was of great help to me and I appreciated it.

I also want to show my appreciation to the PhD students in accelerator physics at the MAX IV Laboratory, Alan, Galina, Joel, Jonas and Olivia, for making me feel a part of the community and giving me a fun time during the work with my thesis.

Most of all, I want to thank my supervisor, Simon C. Leemann, for his support, his very helpful proof-reading of this report and his way of answering all my questions, both the intelligent ones ... and the ones not equally intelligent. Also, I want to thank him for giving me an insight into the wonderful world of accelerator physics and inspiring me to want to learn more in the future.

Table of Contents

Preface - A Brief Introduction to Accelerator Physics 1

1 Introduction 5

2 Background 7
- 2.1 The MAX IV Facility . . . 7
- 2.2 The MAX IV 3 GeV Storage Ring . . . 8
- 2.3 Magnets . . . 10
  - 2.3.1 Magnet Theory 10
  - 2.3.2 Nonlinear Optics of the MAX IV 3 GeV Storage Ring 14
- 2.4 Resonances and Instabilities . . . 16
  - 2.4.1 Optical Resonances 16
  - 2.4.2 Beam Instabilities 19
- 2.5 Optimisation of Nonlinear Optics . . . 22
  - 2.5.1 Chromaticity Correction in Storage Rings 22
  - 2.5.2 Optimisation of Sextupole Magnets 23
  - 2.5.3 Optimisation of Octupole Magnets 27
- 2.6 Performance Measures . . . 29
  - 2.6.1 Dynamic Aperture 29
  - 2.6.2 Momentum Acceptance 31
  - 2.6.3 Touschek lifetime 31

3 Purpose and Methodology 35
- 3.1 Problem Formulation . . . 35
- 3.2 Methodology . . . 36
  - 3.2.1 Overview of the Design Process 36
  - 3.2.2 Simulation Codes 36
  - 3.2.3 Tayloring in OPA 37
  - 3.2.4 Verification of OPA results with Tracy-3 39
  - 3.2.5 Frequency Map Analysis 39

3.2.6 Touschek Tracking 40
3.2.7 Error Studies 41
3.2.8 Technical Limitations 41

4 Results 43
4.1 Nonlinear Optics for High-chromaticity Optics 43
4.2 Chromatic Tune Shifts 44
4.3 Amplitude-dependent Tune Shifts 46
4.4 Dynamic Aperture 48
4.5 Momentum Acceptance 51
4.6 Touschek Lifetime 54
4.7 Error Studies 55
4.8 Technical Limitations 59

5 Discussion and Conclusions 65
5.1 Performance of the High-chromaticity Optics 65
5.2 Challenges for a High-chromaticity Optics 67
5.3 The Design Process 68
5.4 Technical Limitations 69
5.5 Conclusions 69

6 Further Work 71

References 73

Preface - A Brief Introduction to Accelerator Physics

The purpose of this preface is to give a brief introduction to the concepts and terminology used in this report. The principles of particle accelerators and especially storage rings are introduced. This preface also presents the aspects of beam dynamics that are of importance for the understanding of this thesis. For a more in-depth description, an introductory textbook in accelerator physics is recommended, for example [1].

The basic principle of a particle accelerator is to accelerate and guide charged particles with electromagnetic fields. In most accelerators, electric fields are used for acceleration and magnetic fields for guiding. A storage ring is a circular accelerator used for storing a particle beam over prolonged periods of time [1]. The focus of this thesis lies on the MAX IV 3 GeV storage ring, which is a storage ring for electrons with the purpose of producing synchrotron radiation for science [2], and therefore this type of accelerator will be the topic of this preface.

According to the laws of electrodynamics, a charge undergoing acceleration will radiate energy in the form of electromagnetic waves, called synchrotron radiation. Thus, when electrons are circulating in a storage ring they lose energy as synchrotron radiation. An electron storage ring therefore has cavities where radiofrequency fields transfers energy to the electrons to compensate for this energy loss. The storage ring also includes various types of magnets for guiding and focusing of the beam [1]. The elements of the storage ring are placed in a pattern along the ring called lattice. To avoid collisions with gas particles, resulting in the loss of particles from the beam, the beam needs to be travelling in a vacuum pipe with a high vacuum [3]. The electrons are injected into the storage ring during an injection process [1].

A radio frequency (RF) cavity is a resonant cavity fed with a time-varying electromagnetic field. When the particles of the beam enter the

cavity energy is transferred from the RF field to the particles and the particles are accelerated. Due to the time-varying nature of the field the beam gets bunched and this affects the dynamics of the beam [1].

The beam in a circular accelerator is directed on a circular orbit in the horizontal plane by dipole magnets. For every machine an ideal orbit is defined along which a particle with the ideal energy and ideal initial position travels. This orbit is designed to be a closed orbit and is usually located close to the centre of the vacuum chamber of the machine. In reality, the particles of a bunch are spread around the ideal orbit and at a given moment a particle may deviate in both position and angle compared to the ideal orbit. Therefore there is a need for focusing particles back to the ideal orbit to prevent particle loss [3].

The focusing is achieved with quadrupole magnets. The use of quadrupole magnets causes focusing of the beam in one plane while at the same time defocusing in the other plane [1]. Therefore, in order to focus the beam in both planes, focusing and defocusing quadrupoles need to be inserted in an alternating sequence often referred to as a FODO-lattice, for focusing - defocusing. The result is that particles conduct oscillations around the ideal orbit referred to as betatron oscillations and described by the so called beta function, β. These betatron oscillations have a minimum near each defocusing magnet and maximum in the centre of the focusing magnets. Since quadrupole magnets cause different behaviour in the two transverse planes there will be a different beta function for each of the planes. The beta function can be used to determine the amplitude of the oscillations and is therefore commonly used for describing the behaviour of the transverse oscillations of the particles [3].

An important property of a particle beam is the emittance. The emittance is a quality factor of a beam as it indicates how far away from the ideal orbit beam particles oscillate. A small emittance is desired in most rings since this leads to highest brightness or luminosity. The amplitude of the transverse oscillations can be calculated with the use of the emittance and the beta function as $\sqrt{\varepsilon\beta}$, where ε is the constant emittance and β the beta function at that position. The emittance can therefore be used to determine the beam size [1].

As in the transverse plane, particles also conduct oscillations in the longitudinal plane due to the momentum spread of the beam and the bunching and focusing of the RF cavities. The ideal particle with the design energy always arrives at a phase called the synchronous phase where the particle is given exactly the amount of energy from the RF cavities needed to remain on the same orbit [3]. For high-energy storage rings, where the particles have relativistic velocity, particles with a lower momentum travel along a shorter orbit due to stronger bending in the dipole magnets. This means they will

arrive at the RF cavity earlier and see a larger accelerating field than the ideal particle, resulting in a longer orbit during next revolution. The opposite occurs to particles with a higher momentum. The result is that particles oscillate around the synchronous phase and these oscillations are therefore called synchrotron oscillations [1].

Both for betatron and synchrotron oscillations a tune can be defined that describes the number of oscillations per revolution in the machine [3]. The tunes of the machine can change for various reasons, for example because of magnetic field errors or because of large oscillation amplitudes caused by nonlinear motion of the particles. It is important to have knowledge of these tune shifts since they can cause the beam to become unstable, resulting in beam loss [1].

For all accelerators, instabilities are an important issue and need to be avoided in order not to lose the beam. Instabilities can also limit the lifetime of the beam which is of great importance for storage rings since they have the purpose of storing beam over prolonged periods of time. Instabilities cause the amplitude of a particle trajectory to grow uncontrollably. In this context it is necessary to discuss the rise of resonances. It can be shown that for specific values of the tune a resonance can occur as the beam receives a kick at the same phase at every revolution and the amplitude therefore grows continually. Values of the tunes for which resonances occur give rise to so called resonance lines, and strong resonance lines need to be avoided [1].

As mentioned earlier, except for having a spacial deviation from the ideal particle in the transverse and longitudinal planes the particles can also have a momentum deviation. This gives rise to a new closed orbit due to a difference in bending radius in the dipole magnets. This is called dispersion and is described by the dispersion function η. The momentum deviation also gives rise to a difference in focusing from the quadrupole magnets, called chromaticity [3]. The chromaticity and its impact on the performance of the machine is the focus of this thesis and will be discussed in more detail later. The chromaticity caused by the ideal linear optics (dipole and quadrupole magnets) is called natural chromaticity and is corrected by inserting nonlinear optics into the lattice [1]. The reason for this correction and details of how it is performed are also presented in this report.

Another important part of a storage ring used as a light source are the so called insertion devices (IDs). They are inserted into the beam at straight sections in the storage ring to produce synchrotron radiation of high quality that can be used for experiments. They consist of a periodic arrangement of short bending magnets of alternating polarity and cause the electrons to move in a zig-zag pattern leading to the emission of high-brightness synchrotron radiation [1].

Chapter 1
Introduction

The MAX IV facility is a 3rd generation state-of-the-art synchrotron light source currently under construction in Lund, Sweden. The facility will operate a 3 GeV storage ring, which is the focus of this thesis. The MAX IV 3 GeV storage ring has a large negative natural chromaticity in both transverse planes that needs to be corrected to positive values to avoid head-tail instabilities. On the other hand, a large chromaticity can lead to large tune shifts resulting in crossing of potentially dangerous resonances. In the design optics of the MAX IV 3 GeV storage ring the linear chromaticity has therefore been corrected to +1 in both transverse planes to satisfy both the constraint on the sign and on the magnitude of the chromaticity. Initial instability studies show this should be sufficient to avoid instabilities, but since these studies were performed with several approximations there is a need for an alternate optics that can be used if instability issues should occur during commissioning. A short-term solution to these instability issues is to operate the storage ring at a higher chromaticity. The aim of this thesis was therefore to develop an alternate optics for the MAX IV 3 GeV ring with a linear chromaticity of +4 in both planes and to study its performance.

This chapter presented only a brief introduction to the focus of this thesis. Chapter 2 explains the theory required to understand the report. Chapter 3 discusses the focus of this thesis and its motivation in detail. It also presents the methodology that was used during the work. Chapter 4 presents the results of the work. The results are discussed and conclusions drawn in Chapter 5. Ideas for further work are given in Chapter 6.

Chapter 2
Background

2.1 The MAX IV Facility

The MAX IV facility is a state-of-the-art 3rd generation synchrotron light source currently under construction in Lund, Sweden [4]. Synchrotron radiation is produced when charged particles undergo acceleration [1]. In MAX IV electrons will be used as source of synchrotron light [2]. Synchrotron light is useful for experiments in a large number of different fields, e.g. material science, chemistry, biology and medicine [5].

The facility will consist of a 3 GeV linac and two storage rings operated at 3 GeV and 1.5 GeV. The linac will be used as an injector to the storage rings, but also for the production of short X-ray pulses and at a later stage as a driving for a free-electron laser (FEL) [4]. An overview of the facility is given in Fig. 2.1.

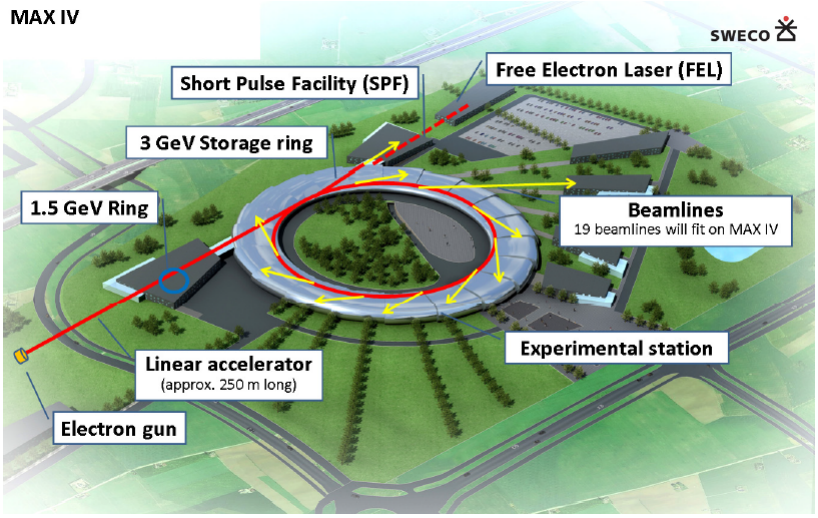

Figure 2.1: An overview of the MAX IV facility [2].

2.2 The MAX IV 3 GeV Storage Ring

The design of the MAX IV 3 GeV storage ring focuses on achieving an ultralow emittance. A 7-bend achromat lattice was chosen for this purpose [6]. An achromat is a magnet structure that consists of several magnet cells and is designed to have no dispersion at its beginning and its end [7]. The MAX IV 3 GeV storage ring consists in total of 20 achromats with seven cells each [6]. A schematic picture of one of the achromats is given in Fig. 2.2. As can be seen, each achromat consists of dipole magnets, quadrupole magnets, sextupole magnets and octupole magnets. The properties of these magnets, with focus on the sextupole and the octupole magnets, are discussed in section 2.3.

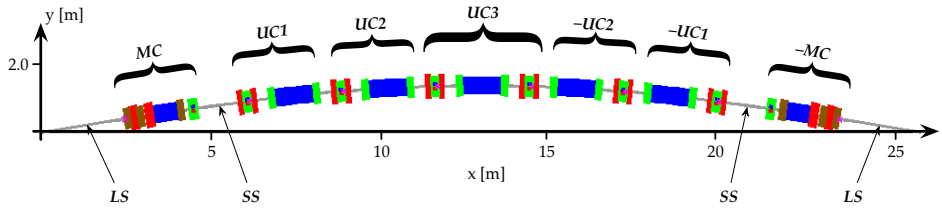

Figure 2.2: A schematic picture of one achromat of the MAX IV 3 GeV storage ring. The achromat consists of dipole magnets (blue), quadrupole magnets (red), sextupole magnets (green) and octupole magnets (brown) [2].

The optical functions for one of the achromats is displayed in Fig. 2.3. The lattice makes use of strong focusing which results in small beta functions and low dispersion leading to a low emittance [2].

Some parameters of interest for the MAX IV 3 GeV storage ring are given in Table 2.1. The design energy of the ring is 3 GeV and the circumference 528 m. The RF frequency of the cavities is 100 MHz and the beam current 500 mA [2]. The harmonic number describes the maximum number of bunches in the beam [3] and is designed to be 176 [2]. The betatron tune is 42.20 in the horizontal plane and 16.28 in the vertical plane [8]. These tunes define the working point, which is the pair of betatron tunes at which the machine is designed to operate [1]. As already mentioned, the ring has a large negative natural chromaticity in both planes which has been corrected to $+1$ in both planes. The momentum acceptance of the lattice is designed to be no less than $\pm 4.5\%$, meaning the lattice is designed to be able to store particles in the interval $\pm 4.5\%$ from the design momentum in the beam [2].

The MAX IV 3 GeV storage ring will use Landau cavities [2] which are harmonic cavities used to improve the lifetime and stability of the beam [9]. The Landau cavities in the MAX IV 3 GeV storage ring will be operated

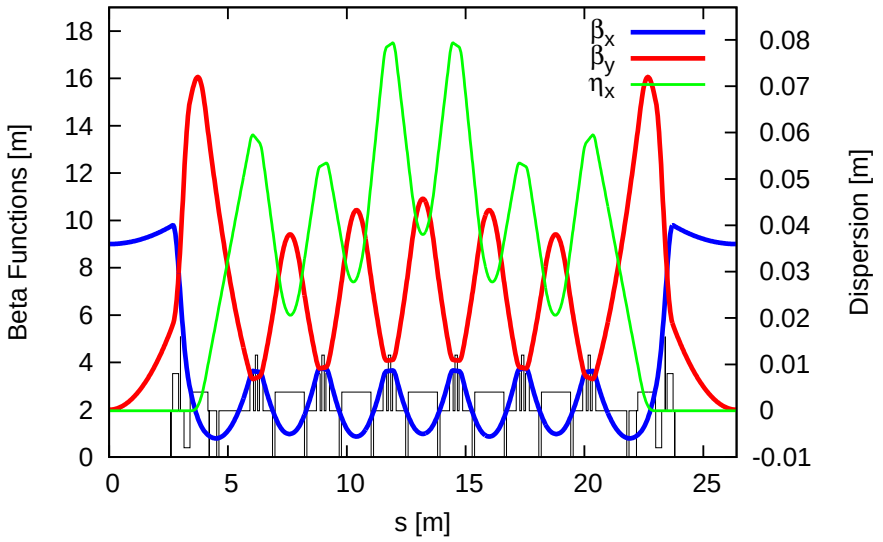

Figure 2.3: Optical functions for one achromat of the MAX IV 3 GeV storage ring. The horizontal beta function β_x (blue) and the vertical beta function β_y (red) are displayed as well as the dispersion function η_x (green). The magnet structure is indicated at the bottom [8].

in passive mode, i.e. without any applied RF voltage, and instead be driven by the electron beam. By tuning the cavity it is possible to achieve bunch lengthening [2] and an increased damping of longitudinal and some transverse oscillations, called Landau damping [9]. Bunch lengthening leads to a decrease in charge density which increases the lifetime of the beam [10]. At the same time, damping of the oscillations leads to damping of instabilities and an improved beam stability [9]. A more thorough description of these effects will be presented in section 2.6.3 and 2.4.2.

Energy [GeV]	3.0 [2]
Main radio frequency [MHz]	99.931 [2]
Harmonic number	176 [2]
Circulating current [mA]	500 [2]
Circumference [m]	528 [2]
Number of achromats	20 [2]
Betatron tune (Horizontal/Vertical]	42.20/16.28 [8]
Natural chromaticity (Horizontal/Vertical)	-49.984/-50.198 [8]
Corrected chromaticity (Horizontal/Vertical)	+1/+1 [2]
Required momentum acceptance	±4.5% [2]

Table 2.1: Design parameters for the MAX IV 3 GeV storage ring

2.3 Magnets

2.3.1 Magnet Theory

The magnetic fields produced by magnets can be derived from Maxwell's equations. A coordinate system (x,y,z) can be defined where x is the horizontal axis, y the vertical axis and z the axis along the beam direction. In a long magnet, the magnetic field can be assumed to be constant along the beam direction and the problem is then reduced to a 2D problem in the xy-plane. The beam will pass at the centre of the magnet and therefore the magnetic field in this area is of interest. Without beam, both the current density and the charge density can be assumed to be zero at the centre of the magnet. The electromagnetic fields can also be assumed to be constant in time [1]. Maxwell's equations are then reduced to

$$\nabla \cdot \mathbf{E} = 0 \tag{2.1a}$$
$$\nabla \times \mathbf{E} = \mathbf{0} \tag{2.1b}$$
$$\nabla \cdot \mathbf{B} = 0 \tag{2.1c}$$
$$\nabla \times \mathbf{B} = \mathbf{0} \tag{2.1d}$$

where $\mathbf{E}$ is the electric field and $\mathbf{B}$ the magnetic flux density [11]. The magnetic field is described by (2.1c) and (2.1d). Since $\nabla \times \mathbf{B} = \mathbf{0}$, the magnetic flux density can be expressed as a scalar potential $\mathbf{B} = \nabla\Phi$ due to $\nabla \times \nabla\Phi = \mathbf{0}$. This gives

$$\nabla \cdot \mathbf{B} = 0 \tag{2.2}$$

$$\Leftrightarrow$$

$$\nabla^2\Phi = 0 \tag{2.3}$$

which is the Laplace equation. By solving the Laplace equation the magnetic field can be determined. An ansatz for the vertical component of the magnetic flux density can be made according to

$$B_y(x,y) = G_y(x) + f(y). \tag{2.4}$$

This means the vertical component of the field can be described by the sum of the vertical component along the horizontal axis $G_y(x)$ and a function $f(y)$ depending on the vertical coordinate. Inserting this ansatz into the Laplace equation gives the potential

$$\Phi(x,y) = G_y(x)y - \frac{1}{6}\frac{d^2G_y(x)}{dx^2}y^3 \tag{2.5}$$

and the magnetic flux density can be calculated according to

$$\mathbf{B}(x,y) = \begin{pmatrix} \frac{d\Phi(x,y)}{dx} \\ \frac{d\Phi(x,y)}{dy} \end{pmatrix}. \tag{2.6}$$

This means that for any given field shape $G_y(x)$ along the horizontal axis the potential and the magnetic field in the transverse xy-plane can be determined [1].

If the vertical component of the magnetic flux density is expanded close to the nominal trajectory along the horizontal direction it becomes

$$\begin{aligned} B_y(x,0) = G_y(0) + G_y'(0)x + \frac{1}{2}G_y''(0)x^2 + \frac{1}{6}G_y^{(3)}(0)x^3 \\ + \frac{1}{24}G_y^{(4)}(0)x^4 + \cdots \end{aligned} \tag{2.7}$$

Hence, the magnetic field can be seen as a sum of multipoles with different effects on the trajectory of the particles. The first term corresponds to a dipole, the second to a quadrupole, the third to a sextupole, the fourth to an octupole etc. When only the two lowest multipoles are used to guide particles in an accelerator this is referred to as linear optics since the forces they give rise to are either constant (dipole) or increase linearly with the transverse deviation from the ideal orbit (quadrupole). The higher order multipoles are referred to as nonlinear optics. However, in reality dipole and quadrupole magnets also give rise to higher order multipoles due to their finite length and magnetic field errors. Therefore, the linear optics in

reality also show nonlinear behaviour. This is usually treated as errors in the machine [1].

The pole shape of the magnets that give rise to the different multipole terms can be derived from the potential in (2.5) and the expansion of the magnetic field in multipoles in (2.7). In this thesis, the focus lies on the nonlinear optics and therefore only the pole shapes of the sextupole and the octupole magnets will be derived here. For a sextupole magnet, the field along the horizontal axis has the form

$$G_y(x) = \frac{1}{2} G_y''(0) x^2 \tag{2.8}$$

according to (2.7). Inserted into (2.5) this gives the potential

$$\Phi(x, y) = \frac{1}{2} G_y''(0) \left(x^2 y - \frac{y^3}{3} \right). \tag{2.9}$$

For a surface of a highly permeable material, such as the iron used in magnet poles, the potential is the same at all points on the surface. This is called an equipotential which means that the potential at the surface of the magnet poles is constant, $\Phi = \Phi_0$. Inserting this into (2.9) gives the shape of the poles as

$$x(y) = \sqrt{\frac{2\Phi_0}{G_y''(0) y} + \frac{y^2}{3}} \text{ [1].} \tag{2.10}$$

The pole profile of a sextupole magnet is displayed in Fig. 2.4. The same derivations for an octupole magnet lead to the pole profile that is displayed in Fig. 2.5.

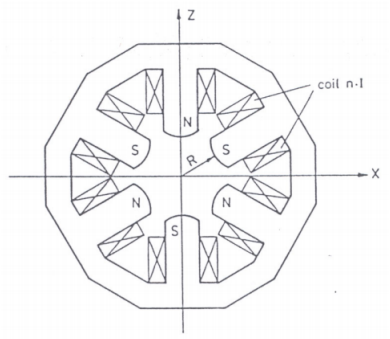

Figure 2.4: Pole profile of a sextupole magnet [12].

However, these potentials and pole profiles do not describe the general solution to the Laplace equation due to the ansatz that was chosen. If a more general ansatz in the form of a Taylor expansion is applied it gives a solution

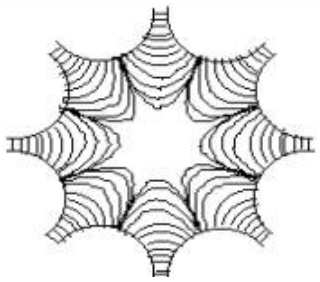

Figure 2.5: Pole profile of an octupole magnet [14].

where the potential has a real and an imaginary part which are two independent solutions to the Laplace equation. These two components differ only in rotational angle. Real magnets used in accelerators are usually aligned such that only one of the two components appears. Unfortunately, the other component can appear as a field error due to misalignment and therefore still has to be considered in a real machine [7]. The magnets can be divided into two types depending on their rotation angle, upright (normal) magnets and rotated magnets, which are also called skew magnets [13]. The fields of the upright magnets for the four types of magnets present in the MAX IV 3 GeV storage ring lattice are given in Table 2.2 and the equivalent fields for the skew magnets in Table 2.3. The pole profile of the skew multipole fields are the same as for the upright fields but rotated around the longitudinal axis with the angle $\frac{\pi}{2n}$, where n is the order of the multipole. An important conclusion from comparing these fields is that the normal linear optics, i.e. upright dipole and quadrupole magnets, do not cause coupling between the particle motion in the horizontal and vertical plane, which is the case for nonlinear optics. This means for normal linear optics the particle motion can be calculated in the two planes independently [7].

Magnet type	Horizontal field	Vertical field
Dipole	$\frac{e}{p}B_x = 0$	$\frac{e}{p}B_y = \frac{e}{p}B_0$
Quadrupole	$\frac{e}{p}B_x = ky$	$\frac{e}{p}B_y = kx$
Sextupole	$\frac{e}{p}B_x = mxy$	$\frac{e}{p}B_y = \frac{1}{2}m(x^2 - y^2)$
Octupole	$\frac{e}{p}B_x = \frac{1}{24}r(3x^2y - y^3)$	$\frac{e}{p}B_y = \frac{1}{24}r(x^3 - 3xy^2)$

Table 2.2: The upright multipole fields [7].

The magnetic strengths are functions of particle momentum and can be denoted according to $\frac{e}{p}B_0 = \frac{1}{R}$, $k = \frac{e}{p}\frac{dB_y}{dx} = b_2$, $m = \frac{e}{p}\frac{d^2B_y}{dx^2} = 2b_3$ and

Magnet type	Horizontal field	Vertical field
Dipole	$\frac{e}{p}B_x = \frac{e}{p}B_0$	$\frac{e}{p}B_y = 0$
Quadrupole	$\frac{e}{p}B_x = -kx$	$\frac{e}{p}B_y = ky$
Sextupole	$\frac{e}{p}B_x = -\frac{1}{2}m(x^2 - y^2)$	$\frac{e}{p}B_y = mxy$
Octupole	$\frac{e}{p}B_x = -\frac{1}{6}r(x^3 - 3xy^2)$	$\frac{e}{p}B_y = -\frac{1}{6}r(3x^2y - y^3)$

Table 2.3: The skew multipole fields [7].

$r = 4\frac{e}{p}\frac{d^3B_y}{dx^3} = 24b_4$ where R is the bending radius, e the electron charge and p the momentum of the particle. Here, the convention $k > 0$ for a horizontally focusing quadrupole magnet is used and the same convention applies to rest of the multipoles. The notations b_3 and b_4 will be used later on for the gradient strengths of sextupole and octupole magnets and is therefore of importance. The expansion of the vertical component of the magnetic flux density close to the nominal trajectory along the horizontal direction in (2.7) with these notations becomes

$$B_y(x,0) = \frac{1}{R} + b_2x + b_3x^2 + b_4x^3 + \cdots \tag{2.11}$$

2.3.2 Nonlinear Optics of the MAX IV 3 GeV Storage Ring

The focus of this thesis is the nonlinear optics of the MAX IV 3 GeV storage ring and therefore the sextupole and octupole magnets will be presented in more detail here. The reason for why the nonlinear optics are of special interest will be explained in section 2.5.

The MAX IV 3 GeV storage ring has five sextupole families. Three of them (SFi, SFo, SFm) are focusing sextupole magnets whereas the other two (SD, SDend) are defocusing sextupole magnets [2]. Their positions in an achromat can be seen in Fig. 2.6. The gradients of the sextupole magnets in the design optics are given in Table 2.4.

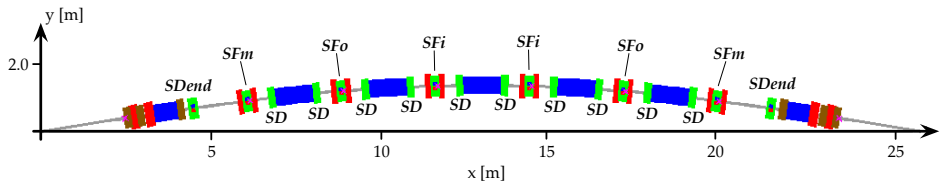

Figure 2.6: The position of the sextupole magnets in an achromat of the MAX IV 3 Gev storage ring [2]

Sextupole family	b_3 [m^{-3}]
SD	-116.625
SDend	-170.000
SFm	170.000
SFo	174.000
SFi	207.412

Table 2.4: The gradients of the sextupole magnets in the design optics of the MAX IV 3 GeV storage ring [8]

The MAX IV 3 GeV storage ring also has three octupole families (OXX, OXY, OYY) [2]. Their position in an achromat can be seen in Fig. 2.7. The gradients of the octupoles magnets in the design optics are given in Table 2.5.

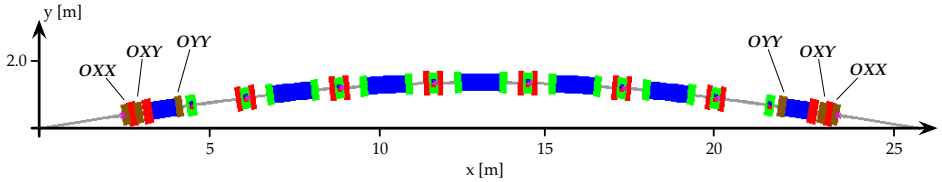

Figure 2.7: The position of the octupole magnets in an achromat of the MAX IV 3 Gev storage ring [2]

Octupole family	b_4 [m^{-4}]
OXX	-1648.58
OXY	3270.14
OYY	-1420.22

Table 2.5: The gradients of the octupole magnets in the design optics of the MAX IV 3 GeV storage ring [8]

2.4 Resonances and Instabilities

2.4.1 Optical Resonances

In a storage ring the beam is affected by the same magnet structure during every revolution while it circulates in the machine. This means that the forces acting upon the beam repeat periodically and under certain conditions the beam can start to resonate. This can lead to growing betatron oscillations and cause the beam to blow up. Sometimes even beam loss can occur if the resonance is sufficiently strong [1].

The phase of the betatron oscillations Φ is defined as

$$\Phi = \oint \frac{dz}{\beta(z)} \tag{2.12}$$

where $\beta(z)$ is the beta function and z the position at the ring. The tune ν describes the number of betatron oscillations during a revolution in the machine and is defined as

$$\nu = \frac{\Phi}{2\pi} \tag{2.13}$$

where Φ is the phase of the betatron oscillation. The equations of motion for a particle travelling through the magnet structure of an accelerator can be used to study the origin of resonances. For a machine with only dipole (with bending radius R) and quadrupole magnets (with focusing strength k), the equations of motion are

$$\begin{cases} x''(z) + \left(\frac{1}{R^2(z)} + k(z)\right) x(z) = \frac{1}{R(z)} \frac{\Delta p}{p} \\ y''(z) - k(z)y(z) = 0 \end{cases} \tag{2.14}$$

where x is the horizontal coordinate, y the vertical coordinate and z the coordinate in the beam direction. These equations describe an ideal machine, but a real machine always has imperfections. The effects of such errors can be studied using a more realistic magnetic field consisting of an ideal magnetic field with added field errors. The field can be expressed as

$$\frac{e}{p} B_y(x,z) = \frac{1}{R} + k(z)x(z) + \frac{\Delta B(x,z)}{RB_0} \tag{2.15}$$

since $\frac{e}{p} = \frac{1}{RB_0}$ according to the motion of a charged particle in a dipole magnet. Setting up the equations of motions for this field gives, for on-momentum particles the inhomogeneous Hill's equation

$$x''(z) + K(z)x(z) = \frac{\Delta B(x,z)}{RB_0}. \tag{2.16}$$

To study resonances the equation can be written in a form which is periodic with the machine circumference. A variable $\phi(s)$ is defined according to

$$\phi(z) = \frac{1}{\nu} \int \frac{dz}{\beta(z)} \tag{2.17}$$

and the transverse amplitude is replaced with by the normalised transverse amplitude

$$\zeta(z) = \frac{x(z)}{\sqrt{\beta(z)}}. \tag{2.18}$$

This will transform (2.16) into

$$\frac{d^2\zeta}{d\phi^2} + \nu^2\zeta = \beta^{3/2}\nu^2 \frac{\Delta B}{RB_0} \tag{2.19}$$

with the solution

$$\zeta(\phi) = \frac{\nu}{2\sin(\pi\nu)} \int_{\phi}^{\phi+2\pi} \beta^{3/2} \frac{\Delta B}{RB_0} \cos(\nu(\pi + \phi + \vartheta))d\vartheta. \tag{2.20}$$

From this solution it becomes clear that the amplitude of the oscillations can grow to infinity as the tune approaches an integer value. While circulating in the machine, if the beam receives a kick from a magnet with a field error and the tune is a whole number, the beam will receive this kick at the same betatron phase every revolution which can result in resonant behaviour [1].

In reality the situation is more complex since all magnets carry imperfections. If the field error $\Delta B(x)$ is expanded in its multipoles and we apply the same transformation of variables as previously used we find the inhomogeneous Hill's equation becomes

$$\frac{d^2\zeta}{d\phi^2} + \nu^2\zeta = \frac{\nu^2}{RB_0}\left(\beta^{3/2}\Delta B + \beta^{4/2}\frac{d\Delta B}{d\zeta}\zeta + \frac{1}{2}\beta^{5/2}\frac{d^2\Delta B}{d\zeta^2}\zeta^2 + \dots\right) \tag{2.21}$$

The first term in this equation describes the effect of a dipole field, the second of a quadrupole field, the third of a sextupole field etc. Solving this equation shows that the dipole term can excite resonances of type $\nu = p$, where p is an integer, whereas the resonance conditions for the quadrupole and the sextupoles terms are $2\nu = p$ and $3\nu = p$, respectively. In the same way higher order resonances can be excited by higher order multipole fields [1].

In a real machine all multipole fields can be present due to technical limitations as well as imperfections and therefore resonances of the type $n\nu = p$, where both n and p are integers, can occur. Since there exist

tunes in the horizontal and vertical planes there exist resonance conditions for both planes. Also, for nonlinear multipole fields the coupling between the particle motion in the horizontal and vertical planes leads to coupling between the betatron oscillations in the two planes and this can result in coupled resonances. The resonance condition for both planes is therefore expressed as

$$n_x\nu_x + n_y\nu_y = p \tag{2.22}$$

where n_x, n_y and p are all integers. The sum $|n_x|+|n_y|$ is called the order of the resonance and in general the strength of the resonance decreases with the order [1]. The optical resonances can be drawn in a diagram such as the one displayed in Fig. 2.8. The resonance lines have different thickness, called stop band width, which is dependent on the strength of the resonance [7]. When choosing a working point for the machine it is important to consider the resonance lines and place the working point far enough from strong resonances to minimize their effect during operation [1].

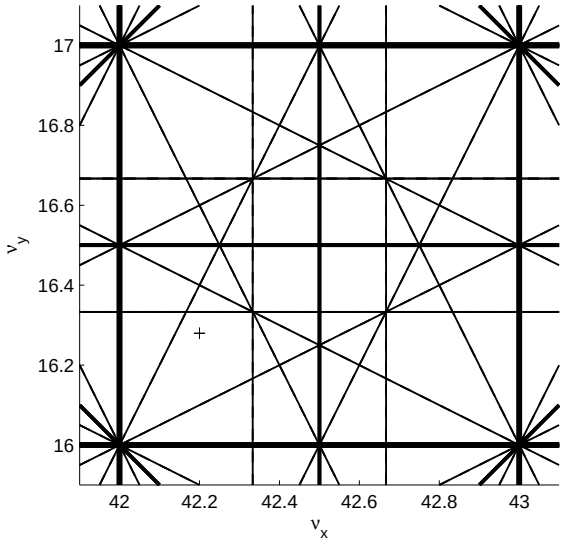

Figure 2.8: Optical resonances up to third order in both transverse planes. ν_x is the horizontal tuned and ν_y the vertical tune. The order is marked by the line width where a thicker line illustrates lower order. The cross in the lower left corner marks a possible working point. Figure inspired by [1].

2.4.2 Beam Instabilities

Beam loss in a machine is not only caused by optical resonances. There are other phenomena that can cause a beam to become unstable. Three types of instabilities of special interest for this thesis will be presented here: the head-tail instability, the transverse mode coupling instability and the resistive wall instability.

Since the beam travels in a metallic vacuum chamber, it will induce image currents in the wall of the chamber. If the chamber were a perfect conductor the electromagnetic fields originating from the image currents would be confined to a narrow longitudinal region around the driving beam particle, but due to the resistivity of the wall the fields are instead spread out, reaching distances far behind the driving particle. The induced fields are called wakefields and can affect either the particle itself or the particles following in the same bunch or in another bunch. Wake fields are also created when the vacuum chamber changes dimensions [7].

Wake fields can change the energy of a single or several particles, which affects the dynamics of the beam and can lead to beam instability. The wake fields can exist for different periods of time, and whereas quickly decaying fields only affect particles in the same bunch, long lasting wake fields can affect particles in the following bunches or even the same bunch after circulation in the machine. The instabilities they give rise to can therefore be divided into single bunch and multi-bunch instabilities. Furthermore, wake fields can be divided into longitudinal and transverse fields which leads to an additional division of the instabilities depending on what type of wake field that causes the instability [7].

The interaction between the beam and the vacuum chamber can be described in both time domain and frequency domain. In the time domain it can be described by wake fields acting on particles in the beam, whereas in the frequency domain the vacuum chamber can be modelled by a frequency-dependent impedance and a beam with a frequency spectrum. If the wall impedance and the beam have components at the same frequency there can exist a coupling and an instability can be driven [7]. As for wake fields, the impedance can be divided into longitudinal and transverse impedances and a certain type of impedance give rise to a certain type of instability. In general the impedances are complex, consisting of a resistive (real) and a reactive (imaginary) part. The resistive part determines the growth of the instability over time, whereas the reactive part determines tune shift and how bunch length changes with beam current [15]. An example of the frequency spectrum of an impedance can be seen in Fig. 2.9. The beam can be described by a similar frequency spectrum where the frequency content is determined by the dynamics of the beam.

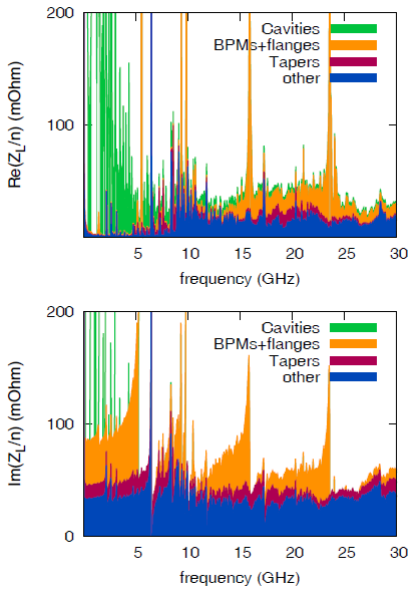

Figure 2.9: Simulated frequency spectrum of the MAX IV 3 GeV geometric longitudinal impedance. The four largest contributors to the impedance are marked [16] .

An instability that is of importance for bunched beams is the head-tail instability. The head-tail instability is caused by transverse wake fields induced by the betatron oscillation of the particles in the head of a bunch, which act on the tail of the same bunch [7] and is thus a single-bunch instability [15]. The frequency of the betatron oscillations depends on the particle momentum and this is, as will be explained in detail in section 2.5.1, described by the so called chromaticity. This means the induced wake fields depend on the chromaticity and therefore also the head-tail instability. It can be shown that for relativistic particles the beam becomes unstable at negative chromaticity at any beam current [7].

The transverse mode coupling instability, also called fast head-tail instability, has the same origin as the head-tail instability, transverse wake fields induced by the head of the bunch affecting the tail of the same bunch. Whereas the head-tail instability can occur at any beam current, the transverse mode coupling instability occurs only when the bunch current exceeds a certain threshold value determined by the impedance of the vacuum chamber. The transverse mode coupling instability therefore limits the possible bunch current in circular accelerators [17]. Initial studies have been performed for the transverse mode coupling instability in the MAX IV 3 GeV storage ring. The threshold bunch current as a function of

chromaticity can be seen in Fig. 2.10. The proposed single-bunch current of the MAX IV 3 GeV storage ring is $500/176 = 2.84$ mA since 500 mA is the total beam current and 176 the harmonic number of the machine. These studies indicate that it is possible to operate the machine with a single bunch current of 2.84 mA at the chromaticity +1 where the ring is designed to operate [18].

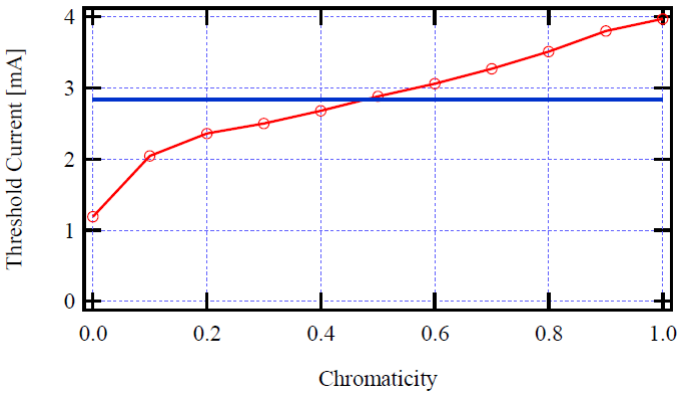

Figure 2.10: Calculated threshold single-bunch current for transverse mode coupling instability as a function of chromaticity. The blue line marks the design single-bunch current for the MAX IV 3 GeV storage ring [18].

Another instability that could limit the possibility of achieving stable operation of the MAX IV 3 GeV storage ring at high beam currents is the resistive wall instability. The resistive wall instability arises from the finite resistivity of the vacuum chamber and is a multibunch instability [15]. The design of the MAX IV 3 GeV storage ring has a compact magnet design which requires small vacuum chamber apertures. This leads to an increase in resistive wall impedance and increased risk for instability [18]. As for the transverse mode coupling instability, initial estimates of the resistive wall impedance of the MAX IV 3 GeV storage ring and its effect on the resistive wall instability have been performed. The threshold current as a function of chromaticity with and without the Landau cavities is displayed in Fig. 2.11. These studies show that the Landau cavities can successfully increase the threshold current for the resistive wall instability. The studies also indicate that it is possible to achieve the 500 mA specified beam current of the MAX IV 3 GeV storage ring without Landau cavities at a chromaticity +1 [18].

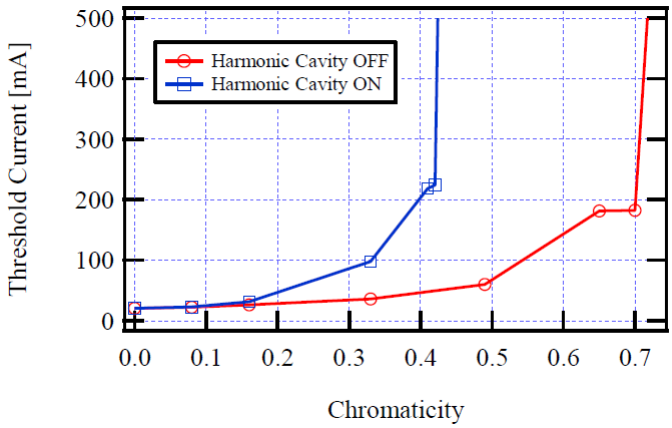

Figure 2.11: Calculated threshold current for the resistive wall instability in the MAX IV 3 GeV storage ring with and without the Landau cavities [18].

2.5 Optimisation of Nonlinear Optics

2.5.1 Chromaticity Correction in Storage Rings

The chromaticity ξ describes the tune shift as a function of momentum deviation and is defined as

$$\xi = \frac{\Delta\nu}{\delta} \tag{2.23}$$

where $\Delta\nu$ is the tune shift and $\delta = \frac{\Delta p}{p}$ the relative momentum deviation [1]. Since the beta function depends on the quadrupole strengths around the machine it can be shown that the chromaticity can be written expressed as

$$\begin{aligned} \xi_x &= -\tfrac{1}{4\pi} \oint k(z)\beta_x(z)dz \\ \xi_y &= \tfrac{1}{4\pi} \oint k(z)\beta_y(z)dz \end{aligned} \tag{2.24}$$

where k is the quadrupole strength and β the beta function [7]. As presented in section 2.3.1, the quadrupole strength is a function of particle momentum which means that off-momentum particles will experience another quadrupole strength than on-momentum particles. This results in different beta functions and according to the definition of tune in (2.13) in tune shift. Thus, quadrupole magnets in the lattice cause chromaticity. From (2.24) it is clear that the influence on the chromaticity is greatest for strong quadrupole magnets placed at positions with large beta function [1].

Modern storage rings used as light sources usually employ strong focusing due to a demand for low emittance [19]. As presented in section 2.4.2,

the head-tail instability arises when the chromaticity is negative. Due to the strong focusing, this is generally the case for the natural chromaticity of all circular accelerators. The strong focusing also gives the natural chromaticity a large magnitude. A large chromaticity means that a small momentum deviation will result in a large tune shift [1]. This can result in beam loss if the tune shift crosses strong resonance lines as stated in section 2.4.2. As detailed in section 2.2, the MAX IV 3 GeV storage ring has a large negative natural chromaticity in both planes. To avoid the head-tail instability and reduce the tune shifts the chromaticity has been corrected to $+1$ in both transverse planes [2]. The reason for correcting the chromaticity to a slightly positive value and not zero is to prevent small variations of the optics to result in negative chromaticity [1]. How chromaticity correction is performed is the topic of the rest of this chapter.

2.5.2 Optimisation of Sextupole Magnets

According to Table 2.2, the vertical component of the magnetic flux density along the horizontal direction for a quadrupole magnet can be described as

$$\frac{e}{p}B_{y,quad} = \frac{e}{p}\frac{dB_y}{dx}x \tag{2.25}$$

and for a sextupoles magnet as

$$\frac{e}{p}B_{y,sext} = \frac{1}{2}mx^2. \tag{2.26}$$

Since

$$\frac{d}{dx}\left(\frac{e}{p}B_{y,sext}\right) = \frac{d}{dx}\left(\frac{1}{2}mx^2\right) = mx \tag{2.27}$$

the field of a sextupole in a small range around a point x_i can be described as a quadrupole with gradient $\frac{dB_y}{dx} = mx$ according to

$$\frac{e}{p}B_{y,quad} = \frac{e}{p}\frac{dB_{y,sext}}{dx} = \frac{e}{p}mxx_i. \tag{2.28}$$

This demonstrates how sextupole magnets can be used to compensate the chromatic effect of quadrupole magnets. The focusing strength of the sextupole magnet depends on the position x_i [19] and correction of the chromaticity can therefore be achieved if the magnets are placed at positions where the particles are sorted by momentum, i.e. at places with dispersion. The particles then have a position x_D according to

$$x_D(z) = \eta_x(z)\delta \tag{2.29}$$

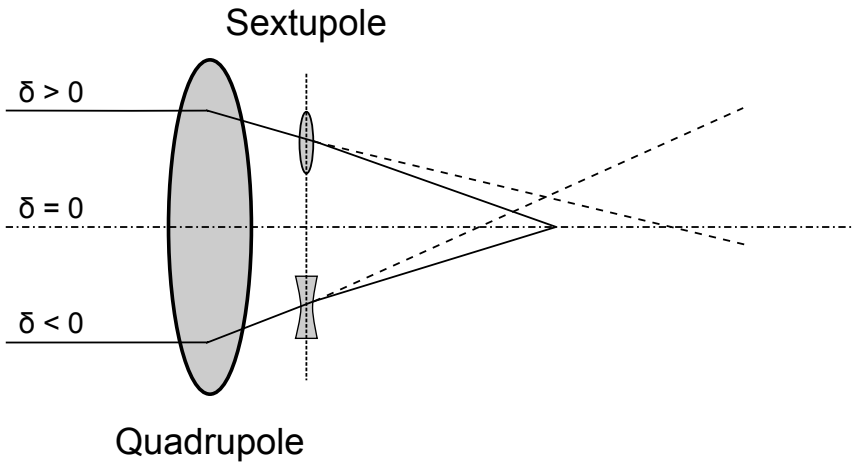

Figure 2.12: Compensation of chromaticity caused by a quadrupole magnet by use of a sextupole magnet. The sextupole magnet focuses particles with a postitive momentum deviation and defocuses particles with a negative momentum deviation. Figure inspired by [1].

where $\eta_x(z)$ is the dispersion function and δ the relative momentum deviation [1]. A schematic figure of such a set up can be seen in Fig. 2.12.

On-momentum particles experience the correct focusing strength of the quadrupole magnets. Since their orbit has no dispersive contribution they will not be affected by the sextupole magnet according to (2.28). Off-momentum particles, however, will experience a weaker or stronger focusing depending on their momentum deviation. Since they are affected by dispersion they will, according to (2.28), be influenced by the sextupole magnet and the strength of the sextupole magnet can be chosen to compensate for the chromatic effect of the quadrupole magnet [1].

To correct both transverse planes, at least two sextupole magnets are required. To correct for focusing quadrupole magnets, focusing sextupole magnets are employed and vice versa for defocusing quadrupole magnets. The corrected chromaticity can be calculated by integrating over the whole ring according to

$$\begin{aligned} \xi_{x,corr} &= \xi_{x0} + \tfrac{1}{4\pi} \oint m(z)\eta_x(z)\beta_x(z) \\ \xi_{y,corr} &= \xi_{y0} - \tfrac{1}{4\pi} \oint m(z)\eta_x(z)\beta_y(z) \end{aligned} \tag{2.30}$$

where ξ_0 is the natural chromaticity, m the sextupole strength, η_x the horizontal dispersion function and β the beta function [7]. If the two sextupole magnets are assumed to have the length l_1 and l_2 and the integral is replaced

with a sum, a system of equations is obtained

$$\begin{aligned} \xi_{x,corr} &= \xi_{x0} + \tfrac{1}{4\pi}(m_1\eta_{x1}\beta_{x1}l_1 + m_2\eta_{x2}\beta_{x2}l_2) \\ \xi_{y,corr} &= \xi_{y0} - \tfrac{1}{4\pi}(m_1\eta_{x1}\beta_{y1}l_1 + m_2\eta_{x2}\beta_{y2}l_2) \end{aligned} . \tag{2.31}$$

By solving this system the sextupole strengths that are required to achieve a certain corrected chromaticity can be found. From these equations it is clear that the required sextupole strength of each magnet can be reduced if the number of sextupole magnets is increased and they are placed at positions with high dispersion. To reduce the required sextupole strength even further, the sextupole magnets with purpose to correct the horizontal plane should be placed at positions with large β_x and low β_y and vice versa for the vertical plane [7].

In general, more than two sextupole magnets are used in a real machine to correct the chromaticity. A way to do this is to arrange the sextupole magnets in families distributed around the ring [7]. As stated in section 2.3.2, the MAX IV 3 GeV storage ring has five sextupole families. Sextupole magnets that are placed in dispersive locations are called chromatic, whereas sextupole magnets that are placed at positions with zero dispersion are called harmonic since they do not affect the chromaticity of the ring [2]. The purpose of harmonic sextupole magnets will be explained later. None of the sextupole magnets in the MAX IV 3 GeV storage ring are purely harmonic so all of them have some effect on the chromaticity depending on the dispersion at their position. Two of the sextupoles families have the main purpose to correct the chromaticity, SFi and SD, since they are the focusing and defocusing sextupole families that are located at positions with highest dispersion, and are therefore the most effective [2].

Unfortunately, sextupole magnets do not only affect the chromatic behaviour of the beam, but can also have negative effects on the beam dynamics. As seen in section 2.4.1, sextupole magnets give rise to resonances. The strength of these resonances can be reduced by adding more sextupole magnets in the lattice which compensate the resonance driving terms caused by the chromatic sextupole magnets. These additional sextupoles do not have to be chromatic, they can be harmonic or installed at very low dispersion. They can suppress the resonances but still keep the chromaticity corrected to the desired value [19].

Sextupole magnets also cause chromatic variation of the beta functions which results in second order chromaticity $\frac{d^2\nu}{d\delta}$. This can lead to large tune shifts for off-momentum particles and can also cause the tune to cross potentially strong resonance lines. Whereas the linear chromaticity can be corrected, the second order chromaticity requires additional effort to compensate for. It can be accomplished by careful tuning of all sextupole magnets

to optimise their strength and position while keeping the linear chromaticity constant [19]. The chromatic tune shifts for the design optics of the MAX IV 3 GeV storage ring can be seen in Fig. 2.13.

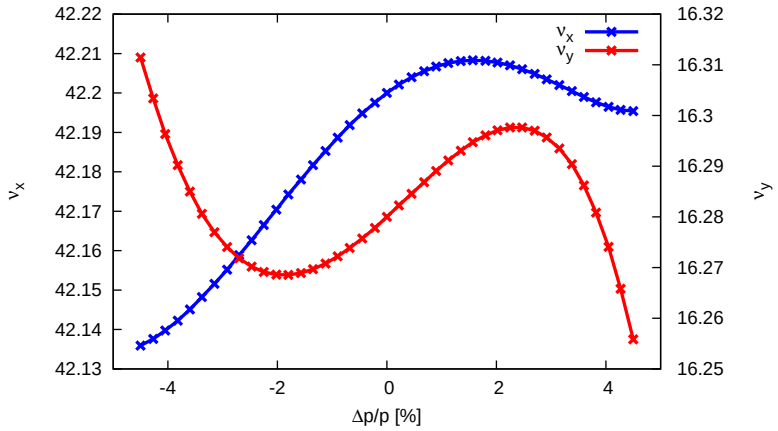

Figure 2.13: Chromatic tune shifts for the design optics of the MAX IV 3 GeV storage ring [8]. As shown by the derivative at $\frac{\Delta p}{p} = 0\%$ the linear chromaticity has been corrected to +1 in both planes.

Even if the second order chromaticity remains large it is possible to tailor the chromatic tune shift to wrap up around the working point and in that way avoid the tune from crossing potentially strong resonance lines [20]. The chromatic tune footprint for the design optics of the MAX IV 3 GeV storage ring where this has been done can be seen in Fig. 2.14.

The sextupole magnets also give rise to amplitude-dependent tune shifts which also can result in crossing of strong resonance lines. As for the second order chromaticity, the amplitude-dependent tune shifts can be reduced by optimising the sextupole magnets. However, since the chromatic tune shift have to be reduced at the same time this can be a difficult task [19].

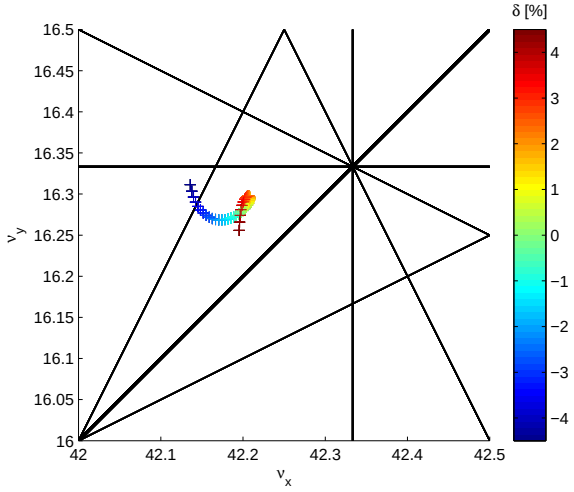

Figure 2.14: The chromatic tune footprint for the design optics of the MAX IV 3 GeV storage ring calculated by OPA. The resonances up to third order are shown. The order is marked by the line width where a thicker line illustrates lower order.

2.5.3 Optimisation of Octupole Magnets

An effective way to compensate for the amplitude-dependent tune shifts caused by the sextupole magnets is to introduce octupole magnets into the lattice. The second order effect caused by the sextupole magnets can then be compensated by octupoles to first order. By optimising the strength and position of the octupole magnets it is possible to tailor and/or minimize these tune shifts. The use of octupole magnets gives more freedom during the design process since it reduces the need for keeping sextupole magnets weak in order not to give rise to large higher-order tune shifts. The sextupole magnets can then be optimised for first-order terms while the octupole magnets are used to compensate for the higher-order terms generated by the sextupole magnets. However, it is important to keep the octupole strength modest in order to prevent strong higher-order terms that in turn needs to be compensated by even higher order magnets [20].

As presented in section 2.3.2, the MAX IV 3 GeV storage ring has three octupole families. Since it was possible to tailor the chromatic tune shifts sufficiently with the sextupole magnets these octupoles were inserted in the lattice with the purpose to reduce the amplitude-dependent tune shifts. They are therefore placed at positions where they will only have a small effect on the chromatic tune shifts [20].

There are four linear amplitude-dependent tune shifts; $\frac{\partial \nu_x}{\partial J_x}$, $\frac{\partial \nu_y}{\partial J_y}$ and

$\frac{\partial \nu_x}{\partial J_y} = \frac{\partial \nu_y}{\partial J_x}$ where ν_x and ν_y are the horizontal and vertical tunes and J_x and J_y are proportional to the horizontal and vertical amplitudes. As for the chromatic tune shift, higher-order amplitude-dependent tune shifts exist as well. These dominate the amplitude-dependent tune shifts at large amplitudes. Only the linear amplitude-dependent tune shifts can be adjusted directly with octupoles. Therefore instead of totally suppressing the linear amplitude-dependent tune shifts, they are adjusted to minimise the overall amplitude-dependent tune shifts across a relevant interval, e.g. the physical acceptance of the machine [20]. The amplitude-dependent tune shifts for the design optics of the MAX IV 3 GeV storage ring can be seen in Fig. 2.15.

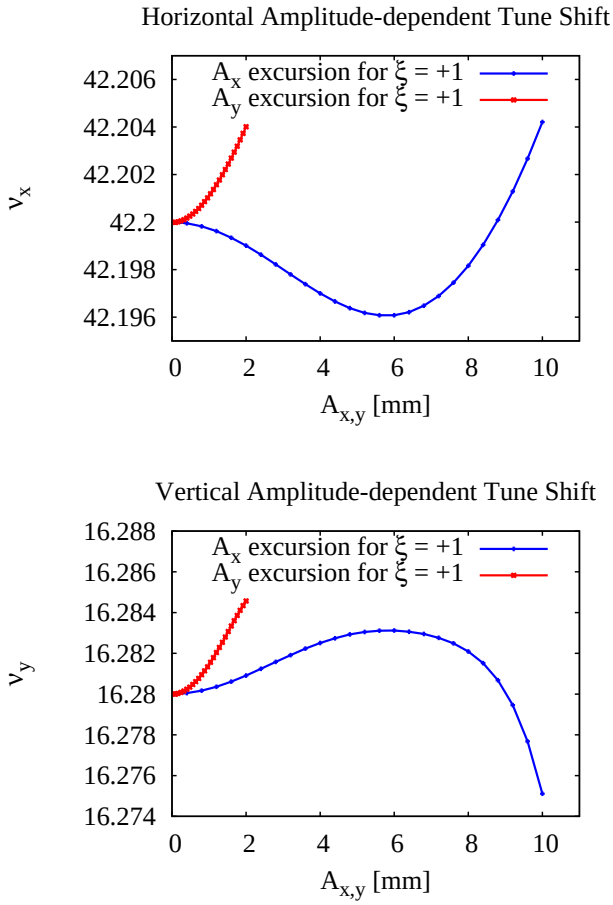

Figure 2.15: The amplitude-dependent tune shifts for the design optics of the MAX IV 3 GeV storage ring calculated by Tracy-3. Figure inspired by [8].

2.6 Performance Measures

2.6.1 Dynamic Aperture

As presented in section 2.5.2, nonlinear behaviour affects the stability of the beam. The motion of a particle can become unstable above certain amplitudes due to amplitude-dependent tune shifts. For off-momentum particles chromatic tune shifts are also of importance. The maximum amplitude at which particle motion remains stable is called dynamic aperture and can vary around the ring [2]. The dynamic aperture in the centre of the long straight sections for the design optics of the MAX IV 3 GeV storage ring is given in Fig. 2.16.

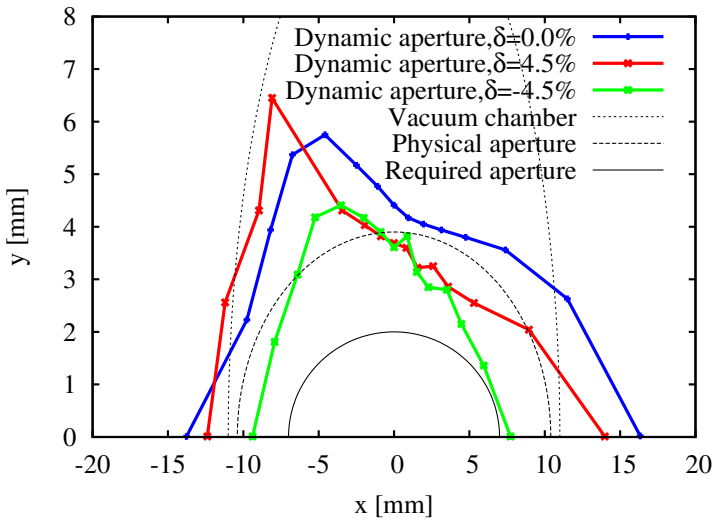

Figure 2.16: The dynamic aperture in the centre of the long straight sections for the design optics of the MAX IV 3 GeV storage ring [8]. The physical aperture corresponds to the physical aperture arising from the vacuum chamber aperture.

Since the beam travels in a vacuum chamber its physical acceptance is limited by the aperture of the vacuum chamber [1]. Ideally the dynamic aperture is as large as the physical aperture but often the dynamic aperture is smaller due to nonlinear effects. The goal of the optics design process is therefore to enlarge the dynamic aperture so it becomes sufficiently large to achieve high injection efficiency and long beam lifetime [2].

The required aperture of the MAX IV 3 GeV storage ring is set by the injection process and insertion devices (IDs). In the horizontal plane the injection process requires around ±5 mm and with error margin the required horizontal aperture has been specified at ±7 mm. In the vertical

plane the IDs limit the physical aperture and therefore a vertical aperture larger than this limit is not required. Including an error margin, the required vertical aperture has been specified at ±2 mm in the centre of the straight sections [21].

The limits for the vacuum chamber, the physical aperture arising from the vacuum chamber and the required aperture for the MAX IV 3 GeV storage ring can be seen in Fig. 2.16. The vacuum chamber has a design inner radius of 11 mm [2]. This limits the physical aperture at the position with the largest beta functions and from this constraint the limit on the physical aperture in the straight sections can be calculated. The amplitude of the betatron oscillations is given by

$$A(z) = \sqrt{\varepsilon\beta(z)} \tag{2.32}$$

where ε is the emittance and β the beta function [1]. The ratio between the amplitude at two different positions along the ring is therefore

$$\frac{A(z_1)}{A(z_2)} = \frac{\sqrt{\varepsilon\beta(z_1)}}{\sqrt{\varepsilon\beta(z_2)}} = \sqrt{\frac{\beta(z_1)}{\beta(z_2)}}. \tag{2.33}$$

The horizontal physical aperture at the straight section can then be calculated according to

$$dx = 11 \cdot \sqrt{\frac{9}{10}} \approx 10.4 \text{ mm} \tag{2.34}$$

since from Fig. 2.3 it can be found that the maximum $\beta_x = 10$ m and $\beta_x = 9$ m at the centre of the straight sections. Similarly, the vertical physical aperture can be calculated to 3.9 mm since the maximum $\beta_y = 16$ m and the value at centre of the straight sections is $\beta_y = 2$ m. Further reduction of the physical aperture occurs at some locations, e.g. because of the septum magnet used during the injection process which limits the aperture of the vacuum chamber to 10 mm at its position [2].

The horizontal required aperture set by the injection process is only valid for on-momentum particles. For off-momentum particles the requirement is less stringent, only enough dynamic aperture to store the particles in the beam is required. According to (2.29) this requires a horizontal aperture of ±3.6 mm for $\delta_{acc} = \pm 4.5\%$ according to

$$dx = \eta_{x,max}\delta_{acc} = 0.08 \cdot \pm 0.045 = \pm 3.6 \text{ mm} \tag{2.35}$$

since from Fig. 2.3 it can be found that the maximum dispersion is 0.08 m.

2.6.2 Momentum Acceptance

The momentum acceptance gives the limit on momentum deviation for when off-momentum particles can no longer be stored in the ring. The source of particles with the largest momentum deviation is the so called Touschek scattering [2]. Touschek scattering refers to collisions between electrons in a bunch where momentum is transferred from the transverse to the longitudinal plane in such a way that the particles are lost [22]. The momentum acceptance can be interpreted as the limit for the maximum momentum transfer in a scattering event not leading to Touschek loss [2].

The RF field in the accelerating cavities sets an upper boundary for the momentum acceptance [2]. This is because particles with a sufficiently large momentum deviation will no longer be in phase with the accelerating field, resulting in unstable synchrotron oscillations [1]. For the RF cavities of the MAX IV 3 GeV storage ring the maximum overall accelerating voltage is 1.8 MV which sets the RF acceptance to $\pm 7.062\%$ [8].

The momentum acceptance is further affected by the dynamic aperture of the lattice since the dynamic aperture varies with momentum [23] and position around the ring [2]. The emission of synchrotron radiation is an essential property of the electron beam in a light source and has not been discussed so far. It is of relevance to consider when discussing the momentum acceptance since the emission of synchrotron radiation leads to loss of momentum and to damping of both betatron and synchrotron oscillations [1]. A Touschek scattered electron travels on a dispersive orbit due to its momentum deviation and oscillates around this orbit. Due to the radiation emission the electron will lose energy along many dispersive orbits while the betatron and synchrotron oscillations are damped. A schematic picture of the electron motion during this damping process can be seen in Fig. 2.17. This means that during the entire damping process, the electron can be lost if it encounters dangerous resonance lines. The variation of dynamic aperture with momentum is therefore of importance for the overall momentum acceptance [2]. The overall momentum acceptance at any location in the lattice is determined as the minimum between the global RF acceptance and the local lattice momentum acceptance [8].

2.6.3 Touschek lifetime

Touschek scattering limits the lifetime of the beam. This is described by the Touschek lifetime. The Touschek lifetime increases with decreased bunch charge density and therefore with increased bunch lengthening. It also depends on several other factors, most importantly, the overall momentum acceptance around the lattice. To determine the Touschek lifetime it is

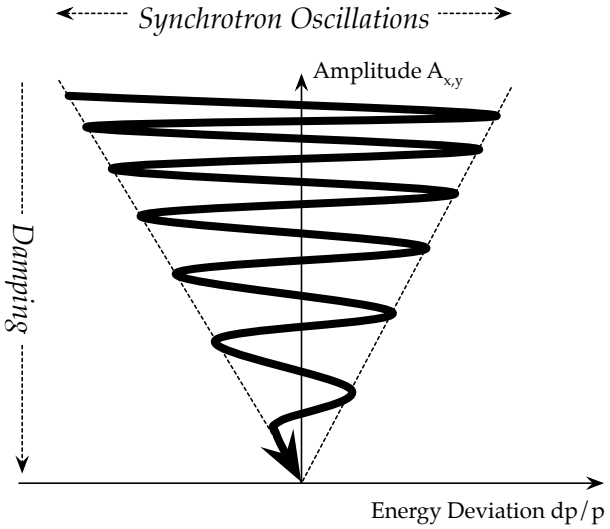

Figure 2.17: Damping process of a Touschek scattered electron [8].

therefore necessary to determine the momentum acceptance at all positions around the ring [2]. The lattice momentum acceptance for one achromat using the design optics of the MAX IV 3 GeV storage ring can be seen in Fig. 2.18.

There are also other phenomena that affect the Touschek lifetime, most importantly intrabeam scattering (IBS) and the Landau cavities. Intrabeam scattering refers to those scattering events that do not result in Touschek loss [24] but do blow up the emittance of the beam and hence increase the Touschek lifetime. The Landau cavities also increase the Touschek lifetime since they lengthen the bunches [8].

The Touschek lifetime has been calculated [8] for the design optics at 500 mA stored current and can be found in Fig. 2.19. These calculations were done without IBS or Landau cavities. With the approximation that the overall momentum acceptance is equal to the RF acceptance and with a maximum cavity voltage of 1.8 MV the Touschek lifetime is around 40 hours. The calculated overall momentum acceptance from tracking with actual vacuum chamber apertures reveals that the Touschek lifetime is reduced to about 14 hours. When the Landau cavities are tuned in the Touschek lifetime increases by roughly a factor 5 [8].

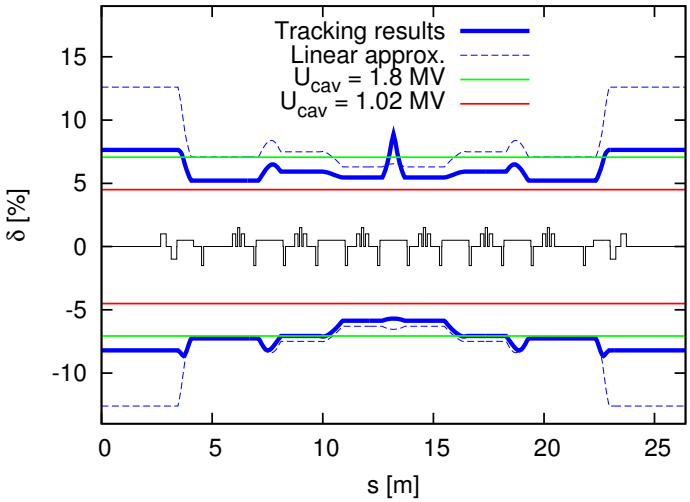

Figure 2.18: The lattice momentum acceptance for one achromat for the design optics of the MAX IV 3 GeV storage ring. The dashed blue line shows a linear optics approximation whereas the solid blue line is the 6D tracking result. The RF acceptance is shown for a maximum cavity voltage of 1.8 MV (green) and for 1.02 MV (red) [8].

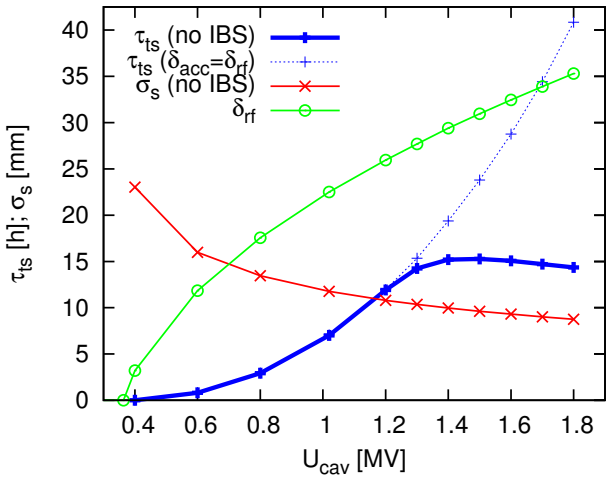

Figure 2.19: Touschek lifetime, bunch length and RF acceptance of the design optics of the MAX IV 3 GeV storage ring as a function of the RF cavity voltage. The stored current was assumed to be 500 mA and the vertical emittance 8 pm rad. The effect of the Landau cavities was not included [8].

Chapter 3
Purpose and Methodology

3.1 Problem Formulation

The goal of this thesis was to develop an alternate optics for the MAX IV 3 GeV ring with linear chromaticity corrected to +4 in both planes and to examine the resulting performance. The initial studies of the transverse mode coupling instability and resistive wall instability presented in section 2.4.2 indicate that the threshold current for both instabilities is beyond what is expected during user operation. However, these studies were performed with several approximations and instability issues might still occur during actual operation. A possible solution is to operate a multibunch feedback system, i.e transverse and/or longitudinal kicker magnets that act on each bunch individually. However, it takes time and effort to implement such a system [25]. Fig. 2.10 and Fig. 2.11 indicate that the threshold current increases with linear chromaticity and a possible short term solution could then be to operate the storage ring at a higher linear chromaticity. This could allow storing larger amounts of current during commissioning, which in turn would allow for further machine studies and development of a long term solution.

The following problem statements were formulated:

- Is it possible to develop an optics with linear chromaticity +4 in both planes for the MAX IV 3 GeV storage ring?
- Is it possible to re-optimize the nonlinear optics of the MAX IV 3 GeV storage ring to achieve the same performance with linear chromaticity +4 as for the design optics with linear chromaticity +1?
- In case this is not possible, what are the resulting differences in performance and which are the factors limiting the performance that can be achieved?

3.2 Methodology

3.2.1 Overview of the Design Process

The methodology used in thesis was an iterative process where a potential candidate for a high-chromaticity optics was developed, analysed and then revised based on the results from the analysis. The aim of this process was to mimick the performance of the design optics. The analysis of the high-chromaticity optics was based on simulations of its performance. The process can be divided into the following steps:

1. Correction of the linear chromaticity to +4 in both planes with the two sextupole families most effective for chromaticity correction, SD and SFi.

2. Tailoring of the chromatic tune shifts using all sextupole families while constraining the linear chromaticity to +4 in both planes.

3. Tailoring of the amplitude-dependent tune shifts by adjusting the octupole families.

4. Study of the on and off-momentum dynamic aperture of the system.

5. Verification of the results by comparison between two different simulation codes.

6. Study of resonant behaviour and limitations of the dynamic aperture with frequency map analysis.

7. Study of beam lifetime with Touschek tracking.

8. Study of the dynamic aperture with errors.

9. Evaluation of technical limitations that might affect the possibility to apply the high-chromaticity optics in the real machine.

3.2.2 Simulation Codes

Two different codes were used for simulations during the design process: OPA and Tracy-3. These codes have different purposes and were useful in different stages of the design process. A brief introduction to their differences and how they were used in this work will be presented here.

OPA is an interactive program with a GUI. It is useful for tailoring the design due to its high interactivity and quick visualisation of results. Its main purpose is the design of electron and positron storage rings and it

includes functionality for sextupole and octupole optimisation. It can calculate chromatic tune shifts and perform tracking in 4D to determine the amplitude-dependent tune shifts and find the dynamic aperture [26]. Tracking is a numerical method where a particle is followed through the magnet structure during a specified number of turns. The elements of the lattice are represented by their transfer matrices and the parameters of the particle by a vector. The initial parameters of the particle are set and it then becomes possible to numerically calculate the parameters after many turns [1]. Detailed information about OPA can be found in the OPA user's manual [26].

Tracy-3 uses more complete models, e.g. 6D tracking, but the calculations take longer time to perform than for OPA. It consists of a library of functions written in C++ that are compiled and run from a terminal. Tracy-3 can be used to calculate the chromatic tune shifts and determine the amplitude-dependent tune shifts and the dynamic aperture by tracking. Unlike OPA, Tracy-3 can also be used to do more advanced analyses, e.g. frequency map analysis, 6D Touschek tracking and error analysis. Detailed information about the basics of Tracy-3 can be found in the user's manual for Tracy-2 [27] since no manual so far exists for Tracy-3.

3.2.3 Tayloring in OPA

Using OPA, the linear chromaticity was corrected to +4 in both planes. The chromatic tune shifts were then tailored by changing the strengths of all sextupole families while constraining the linear chromaticity to +4 in both planes. This was done with a trial-and-error approach with focus on achieving small chromatic tune shifts and at the same time avoiding potentially dangerous resonance lines. The GUI for the sextupole optimization in OPA is shown in Fig. 3.1.

Important to point out is that the changes to the nonlinear optics made in this thesis were done on top of a design optics where the linear optics had already been optimised. The nonlinear optics was thus possible to change without consideration of the linear optics.

The chromatic tune shifts in both planes can be visualised with OPA and were minimised with the chromatic tune shifts of the design optics as reference. OPA can also visualise a tune plot with resonance lines and the tune footprint generated by the chromatic tune shifts. An example of this plot is given in Fig. 3.2. As can be seen, OPA clearly distinguishes between different types of resonances, which facilitates the design process. The chromatic tune footprint was tailored with the priority to avoid lower-order resonances and normal resonances since these were assumed to be potentially most dangerous as they are caused by magnets present in the lattice

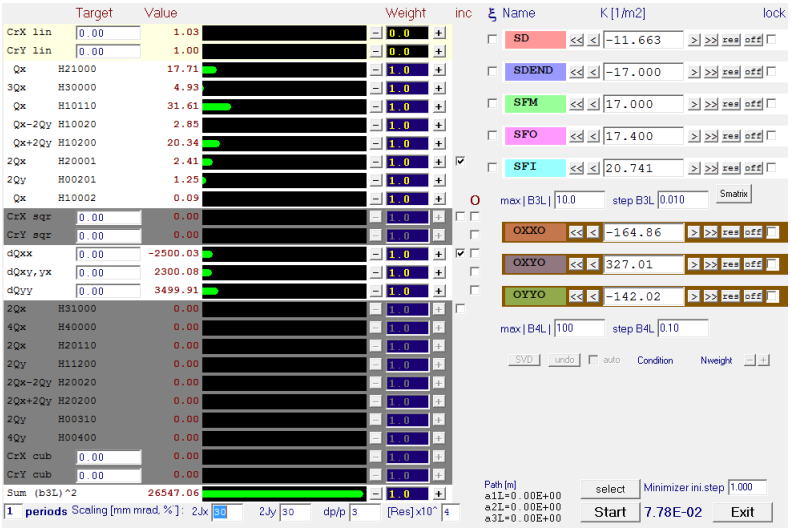

Figure 3.1: GUI of OPA for sextupole optimisation.

and not only by imperfections. During the design process it was learnt that the most effective way to find a good optics was to put focus on tailoring the chromatic tune footprint and then minimise the resulting chromatic tune shifts without causing large changes to the tune footprint, instead of first minimising the chromatic tune shifts and then trying to tailor the chromatic tune shift away from potentially dangerous resonances. Hence, this approach was used during the later stages of the trial-and-error process.

Tracking was performed to determine the amplitude-dependent tune shifts. Desired values for the linear amplitude-dependent tune shifts can be inserted into OPA and a routine returns the required octupole strengths. The values of the linear amplitude-dependent tune shifts were also tailored by a trial-and-error approach with the focus of achieving small overall amplitude-dependent tune shifts within the physical aperture of the machine. During the process the amplitude-dependent tune shifts of the design optics were used as reference.

The dynamic aperture of the high-chromaticity optics was determined by tracking and used to evaluate the results of the tailoring process. The dynamic aperture for on-momentum particles was evaluated as well as the horizontal and vertical dynamic aperture as a function of particle momentum.

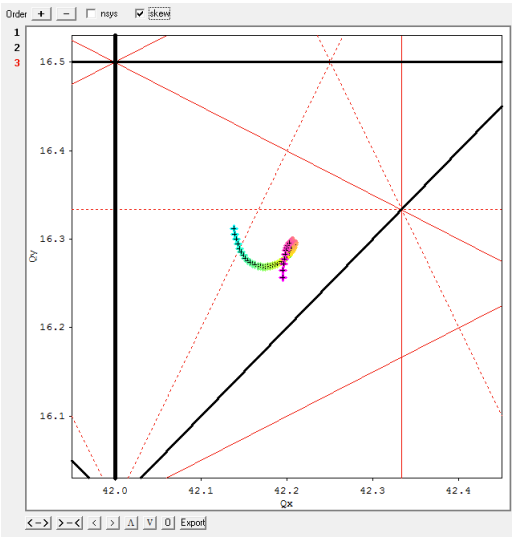

Figure 3.2: Tune plot in OPA showing the chromatic tune footprint and up to third order resonances. The colours indicate how the tune is changed with momentum deviation: blue is negative momentum acceptance and pink positive momentum deviation. Solid lines mark normal resonances and dashed lines skew resonances.

3.2.4 Verification of OPA results with Tracy-3

The results for chromatic tune shifts, amplitude-dependent tune shifts and dynamic aperture obtained by OPA were verified with Tracy-3. This was done to increase the credibility of the results from OPA, but also to find changes to the way Tracy-3 routines are called in order to reproduce the results from OPA.

3.2.5 Frequency Map Analysis

Frequency map analysis was performed to get more information on the dynamics and find where the limitations of the dynamic aperture originate from. This was done both for on and off-momentum particles with Tracy-3.

For a given initial position in the transverse plane and a given momentum a particle is tracked during a certain number of turns. The tunes are derived with a Fast Fourier Transform (FFT) and the diffusion rate calculated according to

$$D = \log \sqrt{\Delta\nu_x^2 + \Delta\nu_y^2} \tag{3.1}$$

where $\Delta\nu_x$ and $\Delta\nu_y$ are the tune shifts between the initial tune and the final tune in the horizontal and vertical planes, respectively [2]. The tune shifts

are calculated by tracking the particle for a number of turns, determining the initial tune, then tracking the particles during the next equal number of turns and determining the final tune. The diffusion rate is a measure of how stable particle motion is. The smaller the diffusion the more stable the motion [28]. From this a diffusion map can be plotted that shows the diffusion rate as a function of initial horizontal and vertical amplitude. The diffusion map can be compared to the dynamic aperture [2].

The diffusion map can be transferred to tune space and a frequency map be obtained [28]. The frequency map describes the diffusion as a function of initial tune [2]. From the frequency map strong resonances can be determined [28] and by linking areas in the diffusion map to areas in the the frequency map it is possible to get information about what limits the dynamic aperture [2]. An example showing how a frequency map can be interpreted is given in Fig. 3.3.

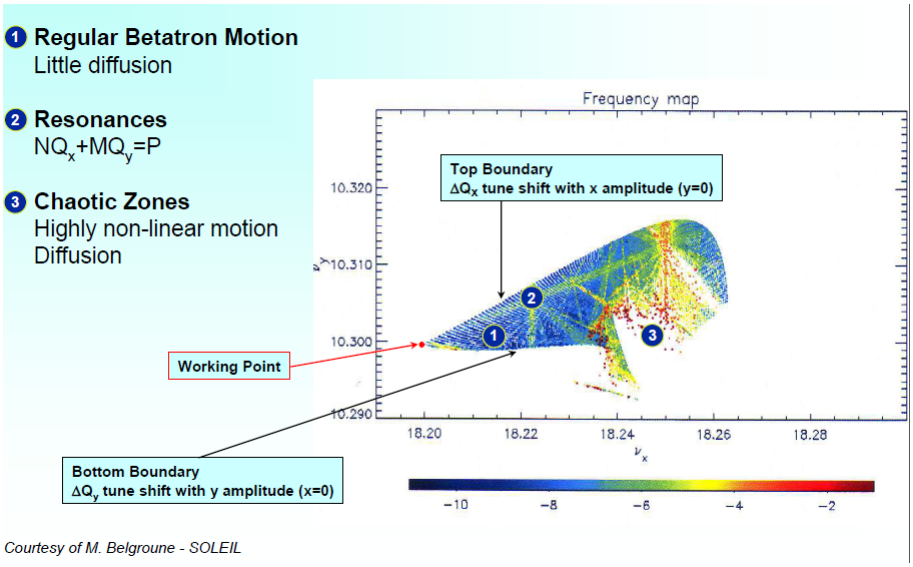

Figure 3.3: Interpretation of a frequency map [28].

3.2.6 Touschek Tracking

The momentum acceptance of the lattice with real physical apertures and the Touschek lifetime were calculated with Tracy-3. First the Touschek lifetime with the approximation that the overall momentum acceptance is equal to the RF acceptance was calculated. Then tracking was performed for the optics with real physical apertures and the lattice momentum acceptance and the overall momentum acceptance at each element around the ring were

determined. From this the Touschek lifetime of the high-chromaticity optics was calculated. The results were verified with OPA.

3.2.7 Error Studies

Error studies were performed to estimate the performance of the high-chromaticity optics in a real machine where it is affected by both systematic and random imperfections, e.g. alignment errors, field errors and multipole errors. The alignment errors are caused by misalignment of the magnets in the machine as well as manufacturing imperfections. Field errors originate from the power supplies and/or mechanical magnet errors whereas multipole errors describe undesired higher-order multipole content of the magnets. The error models were the same as the models used to evaluate the design optics of the MAX IV 3 GeV storage ring and are detailed in [8]. They consist of estimated mean and RMS values for alignment errors, field errors and multipole errors.

The error models were used to determine the dynamic aperture for on and off-momentum with imperfections. This was done by tracking 20 random error seeds using different values for the momentum deviation. In the real machine corrector magnets will be present to correct the orbit [8]. To more closely describe the actual situation in the real machine an orbit correction routine was run before the tracking process. The performance was then evaluated by looking at the resulting reduction of dynamic aperture when errors were present and comparing to the required dynamic aperture.

The reduction of Touschek lifetime due to errors was very roughly estimated by studying the reduction of Touschek lifetime with decreasing RF acceptance while keeping the bunch length constant. Using the approximation that the overall momentum acceptance is equal to the RF acceptance a Touschek lifetime could be calculated and then rescaled to a commom bunch length. Estimates for available lattice momentum acceptance were derived from comparisons of off-momentum dynamic aperture when errors were present.

3.2.8 Technical Limitations

In this thesis the focus lies on the sextupole and octupole magnets of the MAX IV 3 GeV storage ring. It is therefore important to know the technical limitations of these magnets since they might affect the prospect of implementing the results of this work in the real machine. The maximum strength that the magnets are able to produce is of special interest and will therefore be discussed here.

2D simulation models of both the sextupole magnets and the octupole

magnets have been constructed [29]. The simulations of the octupole magnets have been run for different currents to determine the produced magnetic field. The maximum current to the magnets is determined by the power supplies and therefore the power supplies set an upper limit on the achievable magnet strength. If necessary, the power supplies can be replaced in which case the limit is set by the cabling. It is also necessary to take the working temperature of the magnet into consideration. The MAX IV magnet coils are designed to have $dT < 10$ °C at nominal current and if the working temperature exceeds 50 °C the life expectancy of the magnets starts to decrease [30].

In the scope of this thesis, the maximum strengths of the sextupole magnets were simulated in the same way that had previously been performed for the octupole magnets. The previously developed 2D simulations of the sextupole magnets described in [29] were run for different currents to determine the produced magnetic field. The maximum voltage and maximum current specifications of the power supplies detailed in [31] were used to determine the limit on the maximum current possible to achieve from the power supplies. The load on the power supplies, also detailed in [31], were used to determine whether the limit was set by the maximum voltage specification or the maximum current specification of the power supply. Then it was possible to determine the maximum current possible to achieve from the power supplies. The present cabling to the power supplies is also detailed in [31] and the maximum allowable current for this cabling was taken from [32] where the cabling was assumed to be a single conductor placed with a minimum distance of the own outer diameter to the next conductor. The rise of the working temperature was determined with a previously implemented Excel script [33].

Chapter 4
Results

4.1 Nonlinear Optics for High-chromaticity Optics

A candidate for an optics with linear chromaticity +4 in both planes was found with the sextupole gradients given in Table 4.1 and the octupole gradients given in Table 4.2. The gradients for the design optics, presented in section 2.3.2, are given for comparison. The linear amplitude-dependent tune shifts terms were set to $\partial\nu_x/\partial J_x = -3700$, $\partial\nu_y/\partial J_y = 7000$ and $\partial\nu_x/\partial J_y = \partial\nu_y/\partial J_x = 7000$ to minimise the overall amplitude-dependent tune shifts across the physical aperture of the machine.

Sextupole family	Design optics b_3 [m^{-3}] [8]	High-chromaticity optics b_3 [m^{-3}]	Relative difference
SD	-116.625	-109.87	-5.79 %
SDend	-170.000	-250	+47.06 %
SFm	170.000	202	+18.82 %
SFo	174.000	142	-18.39 %
SFi	207.412	217.31	+4.77 %

Table 4.1: The sextupole gradients for the design optics and the high-chromaticity optics.

Octupole family	Design optics b_3 [m^{-3}] [8]	High-chromaticity optics b_3 [m^{-3}]	Relative difference
OXX	-1648.58	-3523.7	+113.74 %
OXY	3270.14	6592.2	+101.59 %
OYY	-1420.22	-3673.3	+158.64 %

Table 4.2: The octupole gradients for the design optics and the high-chromaticity optics.

4.2 Chromatic Tune Shifts

The chromatic tune shift for the high-chromaticity optics in the horizontal plane is displayed in Fig. 4.1 and in Fig. 4.2 for the vertical plane. The chromatic tune shifts for the design optics are also given for comparison. It is clear that for both planes the chromatic tune shift for the high-chromaticity optics are larger than the corresponding tune shift for the design optics.

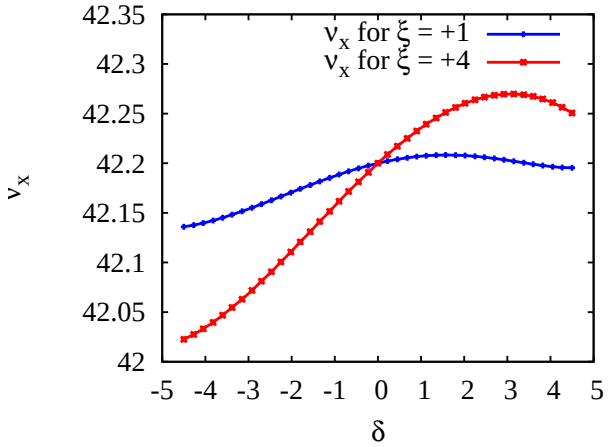

Figure 4.1: The horizontal chromatic tune shift for the high-chromaticity optics calculated by Tracy-3. The horizontal chromatic tune shift for the design optics is given for comparison.

The chromatic tune footprint for the high-chromaticity optics is displayed in Fig. 4.3. As can be seen, the chromatic tune shifts were tailored to avoid the $\nu_x + 2\nu_y = 75$ resonance which is a normal sextupole resonance and thus assumed to be potentially strong. The three resonances, $\nu_x - \nu_y = 26$, $2\nu_x - \nu_y = 68$ and $3\nu_y = 49$ that can be seen crossed by

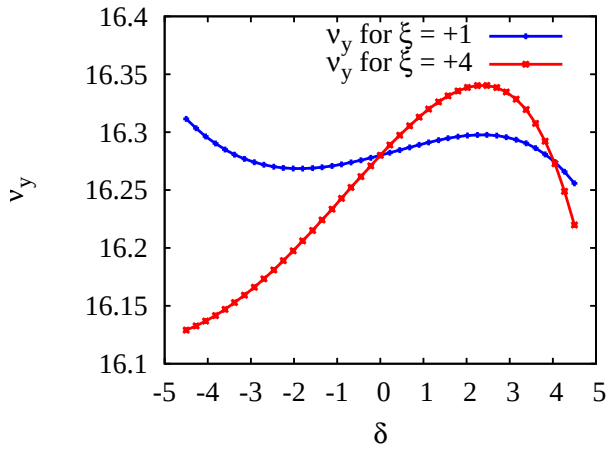

Figure 4.2: The vertical chromatic tune shift for the high-chromaticity optics calculated by Tracy-3. The vertical chromatic tune shift for the design optics is given for comparison.

the chromatic tune footprint are all skew resonances and were therefore assumed to be less strongly driven, and less focus was put on avoiding them during the design process. It is also clear that the chromatic tune footprint for the high-chromaticity optics is much larger than the corresponding tune footprint for the design optics presented previously in Fig. 2.14.

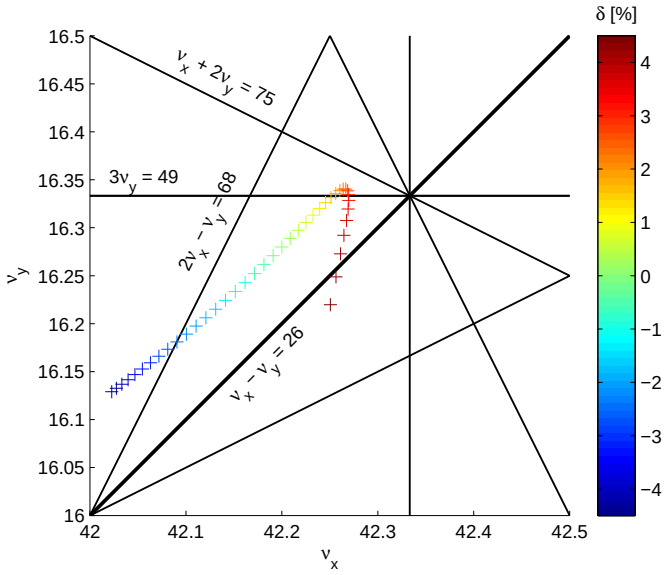

Figure 4.3: The chromatic tune footprint for the high-chromaticity optics calculated by OPA. Resonances up to third order are displayed. The order is marked by the line width where a thicker line illustrates lower order.

4.3 Amplitude-dependent Tune Shifts

The amplitude-dependent tune shifts for the high-chromaticity optics in the horizontal plane are displayed in Fig. 4.4 and in the vertical plane in Fig. 4.5. The amplitude-dependent tune shifts for the design optics are given for comparison.

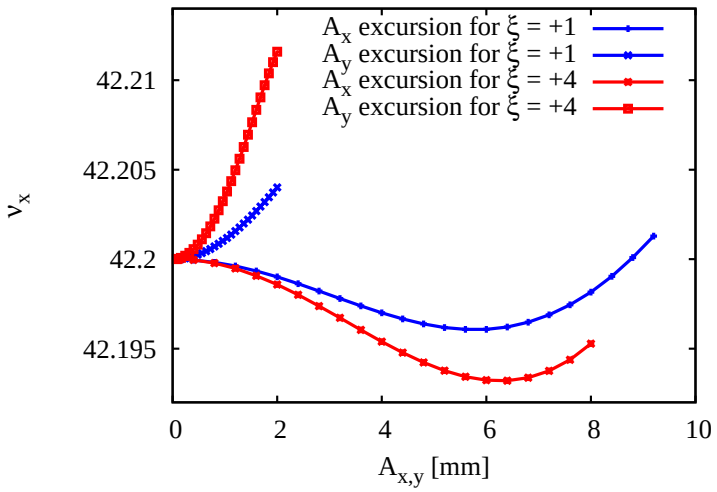

Figure 4.4: The horizontal amplitude-dependent tune shifts for the high-chromaticity optics calculated by Tracy-3. The horizontal amplitude-dependent tune shifts for the design optics are given for comparison.

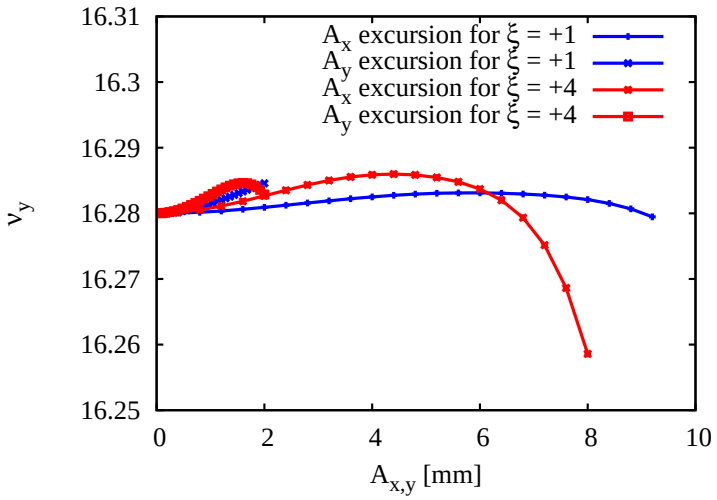

Figure 4.5: The vertical amplitude-dependent tune shifts for the high-chromaticity optics calculated by Tracy-3. The vertical amplitude-dependent tune shifts for the design optics are given for comparison.

4.4 Dynamic Aperture

The dynamic aperture for the high-chromaticity optics can be seen in Fig. 4.6. Comparison with the dynamic aperture for the design optics in Fig. 2.16 shows that the dynamic aperture for the high-chromaticity optics is smaller than the corresponding dynamic aperture for the design optics. Still, the required aperture on-momentum can be fulfilled as well as the requirement off-momentum to be able to store the beam. The dynamic aperture is smaller for $\delta = -4.5\%$ than for $\delta = +4.5\%$ which implies that the reduction of dynamic aperture with momentum deviation is a more serious problem for negative momentum deviations than for positive momentum deviations.

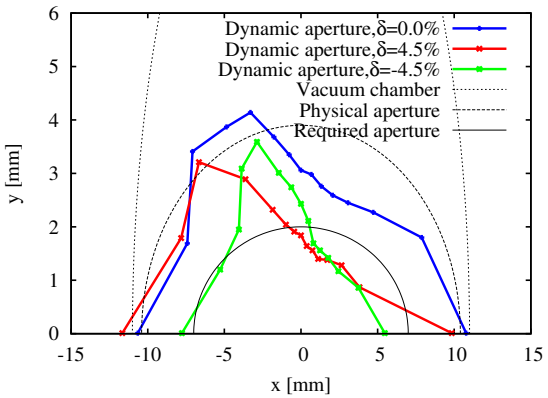

Figure 4.6: Dynamic aperture at the centre of the long straight sections for the high-chromaticity optics calculated by Tracy-3. The physical aperture and the required aperture are also shown.

The diffusion map for on-momentum particles is given in Fig. 4.7 and matches the result for the on-momentum dynamic aperture well. At the core of the dynamic aperture the diffusion is small but it increases towards the boundary of the dynamic aperture. The corresponding frequency map is given in Fig. 4.8. From this frequency map it is not possible to clearly recognise resonances that show a negative effect on the dynamic aperture.

A magnification of the core area of the on-momentum diffusion map is displayed in Fig. 4.9. It can be seen that minor diffusion exists within the required dynamic aperture. Possible resonant behaviour is also visible as ring formed structures with increased diffusion. The corresponding frequency map is displayed in Fig. 4.10. By connecting areas in the diffusion map to areas in the frequency map (marked A, B and C) two resonances were found. These were the normal 5th order resonance $3\nu_x - 2\nu_y = 94$ and the normal 9th order resonance $3\nu_x - 6\nu_y = 29$.

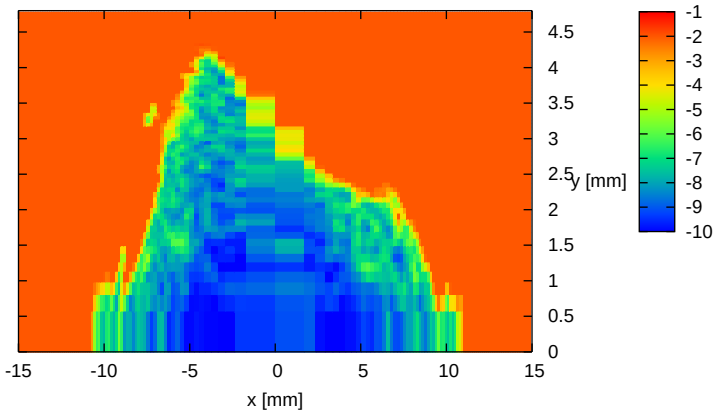

Figure 4.7: Diffusion map for on-momentum particles at the centre of the long straight sections for the high-chromaticity optics calculated by Tracy-3. Blue areas show low diffusion and red areas high diffusion. Tracking has been performed for 2046 turns.

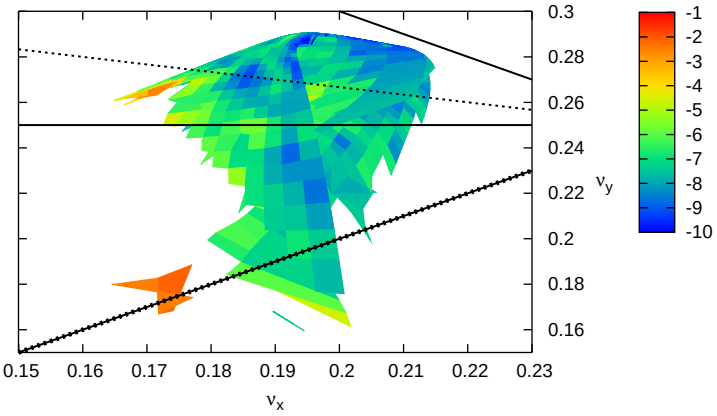

Figure 4.8: Frequency map for on-momentum particles at the centre of the long straight sections for the high-chromaticity optics calculated by Tracy-3. Blue areas show low diffusion and red areas high diffusion. Tracking has been performed for 2046 turns. Resonance lines up to 4th order are indicated: normal (solid) and skew (dotted). The order is marked by the line width where a thicker line illustrates lower order.

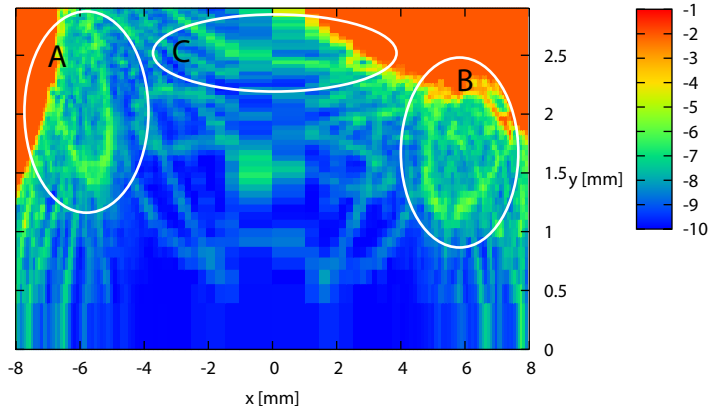

Figure 4.9: Diffusion map for the core area of the dynamic aperture for on-momentum particles at the centre of long the straight sections for the high-chromaticity optics calculated by Tracy-3. Blue areas show low diffusion and red areas high diffusion. Tracking has been performed for 2046 turns. .

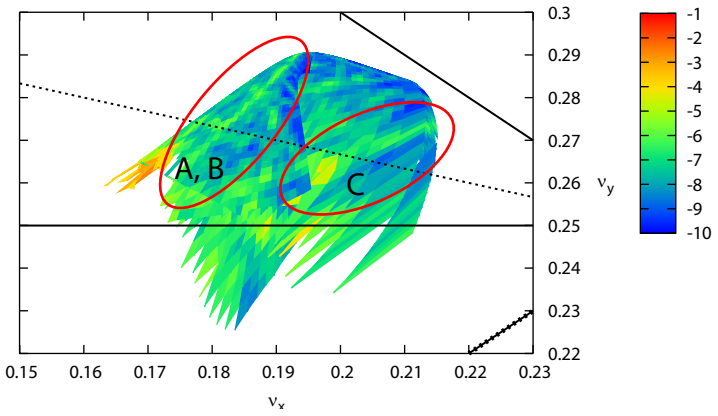

Figure 4.10: Frequency map for the core area of the dynamic aperture for on-momentum particles at the centre of the long straight sections for the high-chromaticity optics calculated by Tracy-3. Blue areas show low diffusion and red areas high diffusion. Tracking has been performed for 2046 turns. Resonance lines up to 4th order are indicated: normal (solid) and skew (dotted).The order is marked by the line width where a thicker line illustrates lower order.

4.5 Momentum Acceptance

The diffusion map for off-momentum particles is displayed in Fig. 4.11. The momentum acceptance appears to be limited to around $\delta = -7\%$ and $\delta = +9\%$. Within the desired momentum acceptance $\delta = \pm 4.5\%$ several areas with elevated diffusion and some bands and ring formed structures indicating resonant behaviour can be seen. The corresponding frequency map is displayed if Fig. 4.12. By connecting areas in the diffusion map to areas in the frequency map (marked A, B and C) two resonances can be recognised, $4\nu_x = 169$ and $4\nu_y = 65$. These are both normal 4th order resonances. These resonances are even better visible in the magnified frequency map displayed in Fig. 4.13. Around $\delta = -5\%$ an area of lower diffusion can be seen at large amplitudes. For $\delta < 5\%$ there seems to be an area with chaotic motion. By connecting this area to the frequency map it can be concluded that this occurs in an area close to the integer resonance.

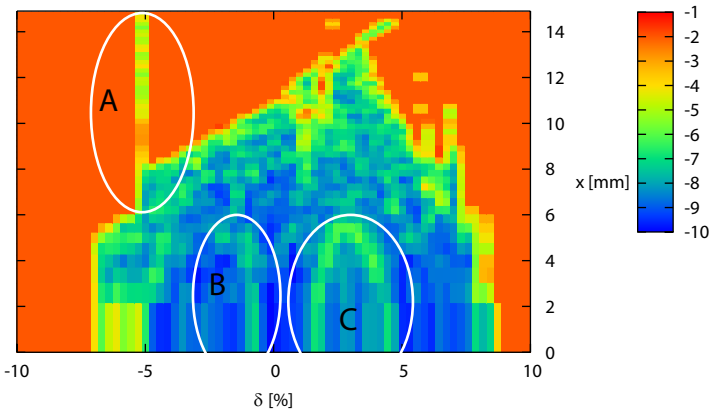

Figure 4.11: Diffusion map for off-momentum particles at the centre of the long straight sections for the high-chromaticity optics calculated by Tracy-3. Blue areas show low diffusion and red areas high diffusion. Tracking has been performed for 2046 turns. The vertical amplitude was set to +0.1 mm.

A magnification of the core area of the off-momentum diffusion map is displayed in Fig. 4.14. The ring formed structures seen in Fig. 4.11 can be recognised. The corresponding frequency map is displayed in Fig. 4.15. The resonances $4\nu_x = 169$ and $4\nu_y = 64$ previouly recognised in Fig. 4.12 are clearly visible.

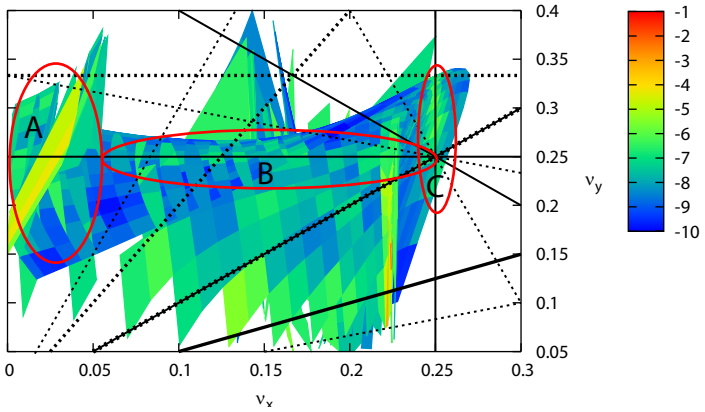

Figure 4.12: Frequency map for off-momentum particles at the centre of the long straight sections for the high-chromaticity optics calculated by Tracy-3. Blue areas show low diffusion and red areas high diffusion. Tracking has been performed for 2046 turns. Resonances up to 4th order are indicated: normal (solid) and skew (dotted). The order is marked by the line width where a thicker line illustrates lower order.

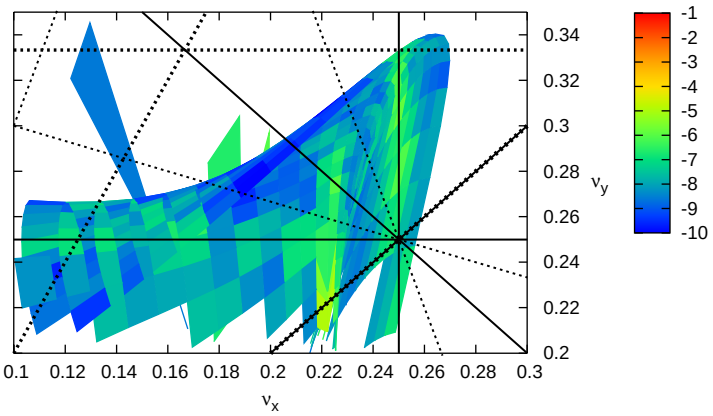

Figure 4.13: Magnified frequency map for off-momentum particles at the centre of the straight sections for the high-chromaticity optics calculated by Tracy-3. Blue areas show small tune shifts and red areas large tune shifts. Tracking has been done for 2046 turns. The resonance lines up to 4th order is marked: upright (solid) and skew (dotted). The order is marked by the line width where a thicker line illustrates lower order.

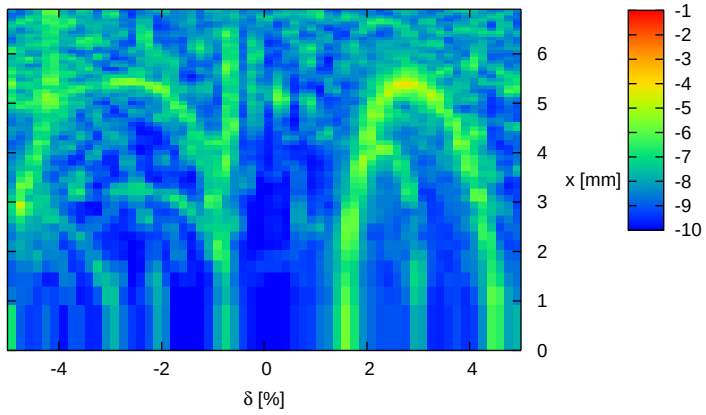

Figure 4.14: Diffusion map for the core area of the dynamic aperture for off-momentum particles at the centre of the long straight sections for the high-chromaticity optics calculated by Tracy-3. Blue areas show low diffusion and red areas high diffusion. Tracking has been performed for 2046 turns. The vertical amplitude was set to +0.1 mm.

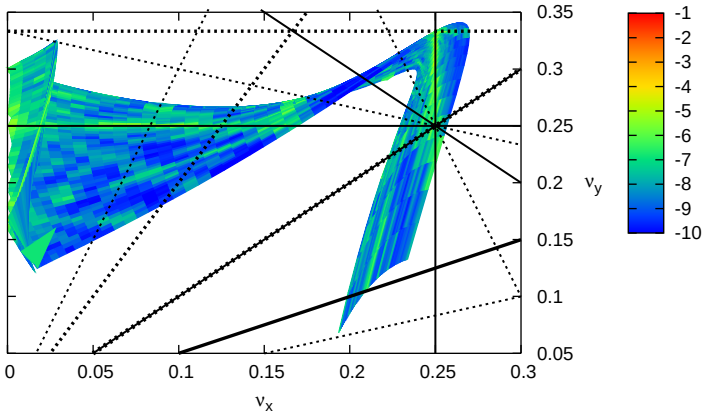

Figure 4.15: Frequency map for the core area of the dynamic aperture for off-momentum particles at the centre of the long straight sections for the high-chromaticity optics calculated by Tracy-3. Blue areas show low diffusion and red areas high diffusion. Tracking has been performed for 2046 turns. Resonances up to 4th order are indicated: normal (solid) and skew (dotted). The order is marked by the line width where a thicker line illustrates lower order.

The overall momentum acceptance for one achromat of the MAX IV 3 GeV storage ring for the high-chromaticity optics can be seen in Fig. 4.16. The overall momentum acceptance was calculated with a maximum RF voltage of 1.8 MV and actual vaccum chamber apertures. Comparison with the RF acceptance and the lattice momentum acceptance for one achromat using the design optics shown in Fig. 2.18 reveals that the momentum acceptance for the high-chromaticity is generally lower than for the design optics. The situation appears especially critical for negative momentum deviations, where the desired momentum acceptance $\delta = -4.5\%$ is just barely achieved.

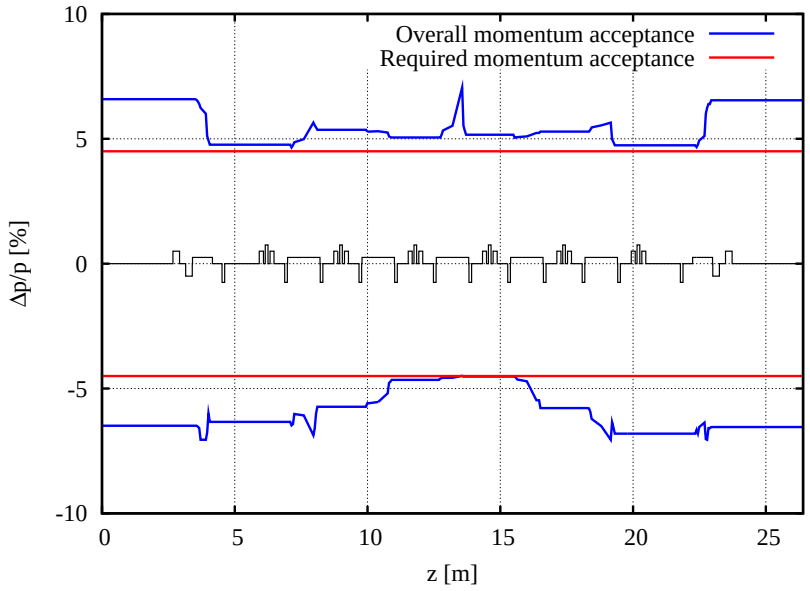

Figure 4.16: Overall momentum acceptance for one achromat of the MAX IV 3 GeV storage ring for the high-chromaticity optics with maximum RF voltage 1.8 MV and actual vacuum chamber apertures. Tracking was done with Tracy-3 for 318 turns. The blue lines shows the overall momentum acceptance and the red lines mark the desired momentum acceptance at $\delta = \pm 4.5\%$. The magnet structure is indicated in black.

4.6 Touschek Lifetime

The Toushek lifetime was determined by Tracy-3 through tracking. For a beam current of 500 mA, a vertical emittance of 8 pm rad and a maximal cavity voltage of 1.8 MV the Touschek lifetime was calculated to 40.86 hours

with the approximation that the momentum acceptance is equal to the RF acceptance. For the overall momentum acceptance with actual vacuum apertures given in Fig. 4.16 and the same parameters on the beam current, vertical emittance and cavity voltage the Touschek lifetime was calculated via 6D tracking in Tracy-3 to 8.98 hours. The effects of the Landau cavities and IBS were not included in either calculation. Comparison with the Touschek lifetimes for the design optics presented in section 2.6.3 reveal that the Touschek lifetime is around 5 hours lower for the high-chromaticity optics.

4.7 Error Studies

The dynamic aperture with errors for on-momentum particles can be seen in Fig. 4.17. Although the dynamic aperture is reduced when errors are introduced, some dynamic aperture still remains. The required horizontal aperture on-momentum is still fulfilled. The dynamic aperture for off-momentum particles can be seen in Fig. 4.18 and Fig. 4.19. The situation for off-momentum particles is significantly poorer than for on-momentum particles. For $\delta = +4.5\%$ the horizontal aperture is far from the ± 3.6 mm calculated in (2.35) and at $\delta = -4.5\%$ there does not remain any dynamic aperture at all.

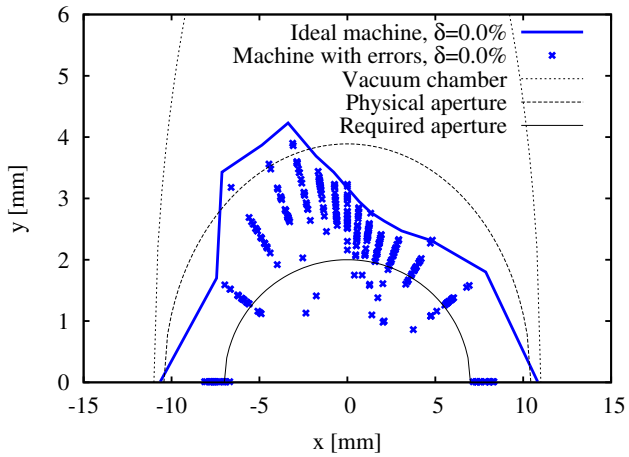

Figure 4.17: The dynamic aperture at the centre of the long straight sections on-momentum for the high-chromaticity optics with field, multipole and alignment errors. Tracking was performed for 20 seeds with Tracy-3.

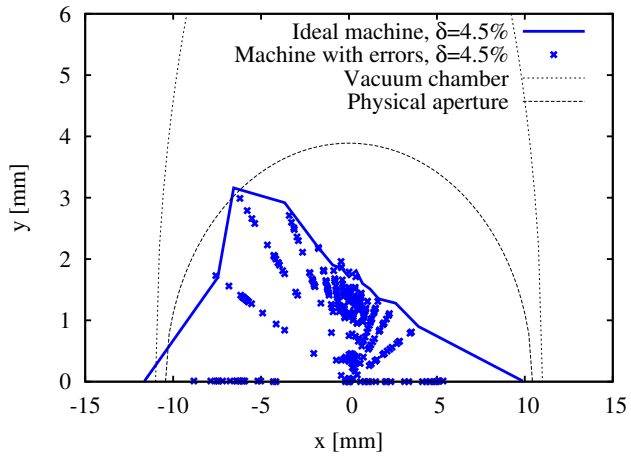

Figure 4.18: The dynamic aperture at the centre of the long straight sections for $\delta = +4.5\%$ for the high-chromaticity optics with field, multipole and alignment errors. Tracking was performed for 20 seeds with Tracy-3.

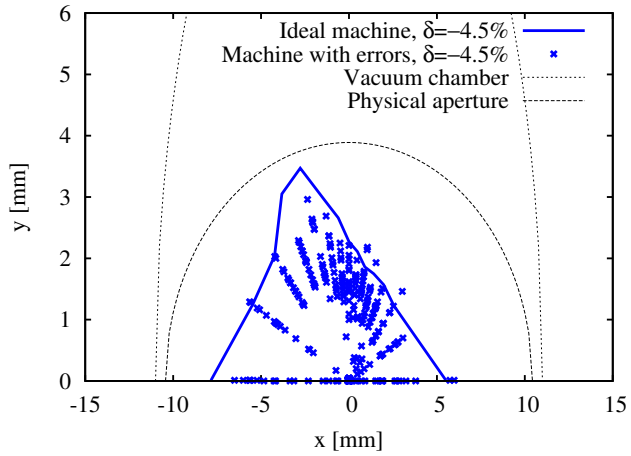

Figure 4.19: The dynamic aperture at the centre of the long straight sections for $\delta = -4.5\%$ for the high-chromaticity optics with field, multipole and alignment errors. Tracking was performed for 20 seeds with Tracy-3.

The dynamic aperture for $\delta = 4\%$ can be seen in Fig. 4.20 and for $\delta = 3.5\%$ in Fig. 4.21. It is clear that the dynamic aperture is larger for particles with lower momentum deviation.

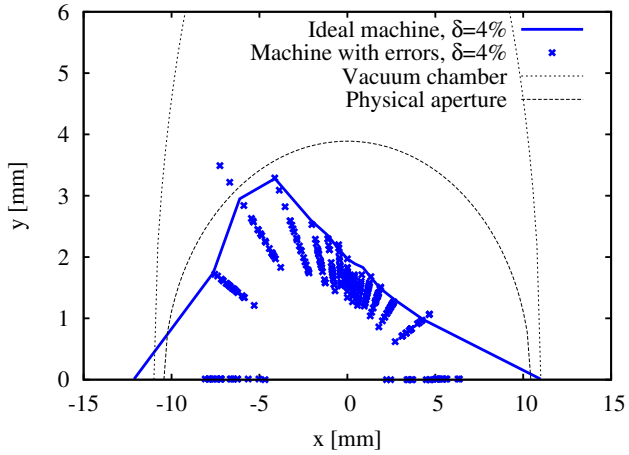

Figure 4.20: The dynamic aperture at the centre of the long straight sections for $\delta = +4\%$ for the high-chromaticity optics with field, multipole and alignment errors. Tracking was performed for 20 seeds with Tracy-3.

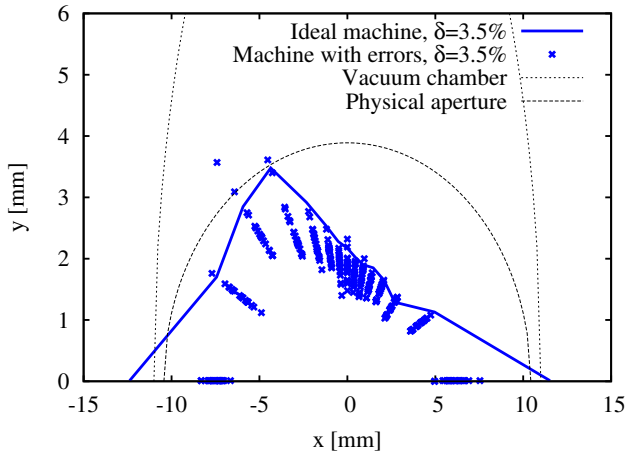

Figure 4.21: The dynamic aperture at the centre of the long straight sections for $\delta = +3.5\%$ for the high-chromaticity optics with field, multipole and alignment errors. Tracking was performed for 20 seeds with Tracy-3.

The dynamic aperture for $\delta = -4\%$ can be seen in Fig. 4.22 and for $\delta = -3.5\%$ in Fig 4.23. It is apparent that the reduction of the dynamic aperture due to errors is more dramatic for negative momentum deviations than for positive momentum deviations.

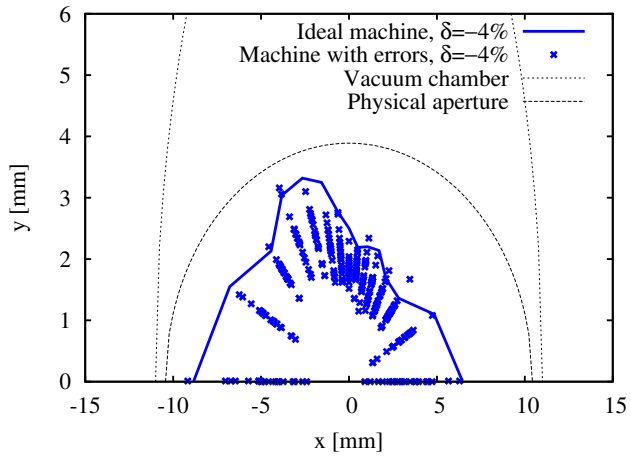

Figure 4.22: The dynamic aperture at the centre of the long straight sections for $\delta = -4\%$ for the high-chromaticity optics with field, multipole and alignment errors. Tracking was performed for 20 seeds with Tracy-3.

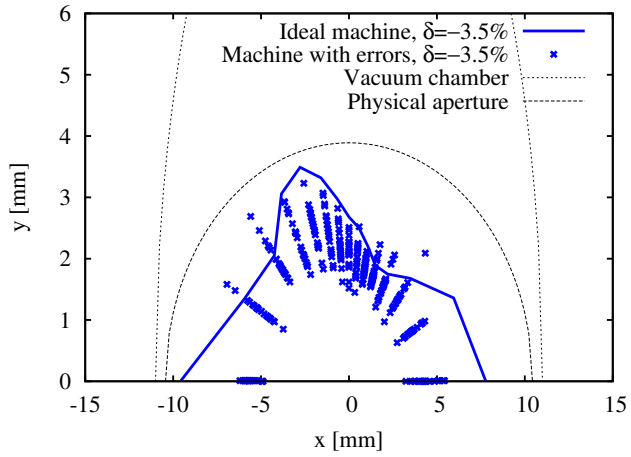

Figure 4.23: The dynamic aperture at the centre of the long straight sections for $\delta = -3.5\%$ for the high-chromaticity optics with field, multipole and alignment errors. Tracking was performed for 20 seeds with Tracy-3.

The reduction of Touschek lifetime due to the reduction of momentum acceptance was very roughly estimated by studying the Touschek lifetime acquired with the approximation that the overall momentum acceptance is equal to the RF acceptance. The Touschek lifetime for different RF ac-

ceptances was determined by OPA and then rescaled to match the bunch length at a maximum cavity voltage of 1.8 MV. In this way the Touschek lifetime at a maximum cavity voltage of 1.8 MV but with a reduced overall momentum acceptance could be roughly estimated. The Touschek lifetimes are given in Table 4.3. If the overall momentum acceptance is reduced to $\pm 3.5\%$ this gives a Touschek lifetime of around 2 hours. However, the reduction to $\delta = \pm 3.5\%$ is only valid in the centre of the long straight sections and, as is displayed in Fig 4.16 this is not the position with the lowest lattice momentum acceptance. To get a very rough estimate of how poor the momentum acceptance with errors can become, the dynamic aperture with imperfections was studied in the centre of the achromat for negative momentum deviations since according to Fig. 4.16 this is the location with the lowest lattice momentum acceptance. These studies reveal that the lattice momentum acceptance in the centre of the achromat with errors present is expected to be between -2% to -3%.

Maximum cavity voltage [MV]	RF acceptance [%]	Natural bunch length [mm]	Touschek lifetime [h]	Rescaled Touschek lifetime [h]
1.8	7.062	8.81	40.613	40.613
1.02	4.501	11.98	7.088	5.212
0.91	4.031	12.80	4.8	3.304
0.8	3.511	13.85	3.0	1.908
0.62	2.501	16.50	1.016	0.542
0.56	2.096	17.92	0.599	0.294
0.48	1.467	20.90	0.219	0.092

Table 4.3: Touschek lifetimes for the approximation that the overall acceptance is equal to the RF acceptance calculated by OPA. The lifetimes have also been rescaled to the bunch length at a maximum cavity of 1.8 MV.

4.8 Technical Limitations

The simulations of the gradient strengths for the sextupole magnets are displayed in Fig. 4.24 - Fig. 4.28. For none of the magnets the limit $dT < 10$ °C on the working temperature was exceeded for currents up to the maxi-

mum defined by the cabling. The saturation of the magnets can be seen in the figures since the derivate between two simulation points decreases for higher currents, going towards an asymptotic behaviour. Fig. 4.25 shows that the gradient strength required for the high-chromaticity optics cannot be achieved for the SDend magnets with present power supply, but present cabling is sufficient. For all other magnets the required gradient strengths for the high-chromaticity optics should be available with the present power supplies.

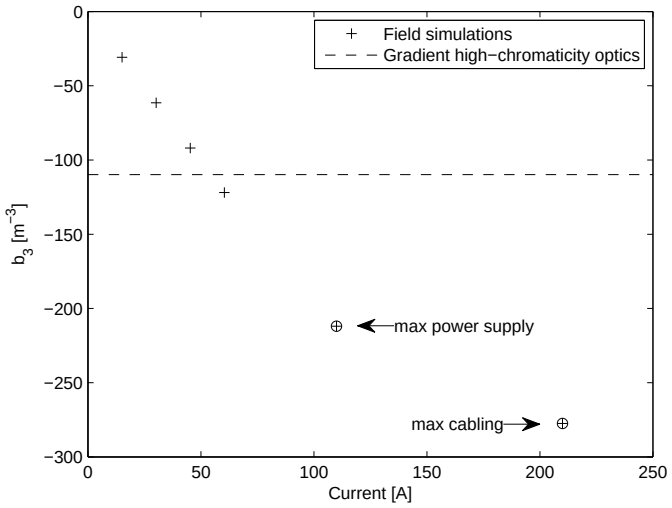

Figure 4.24: Simulated gradient strength as function of current for the SD magnet. The maximum gradient that can be produced with the present power supply and cabling is marked, as well as the gradient strength needed for the high-chromaticity optics.

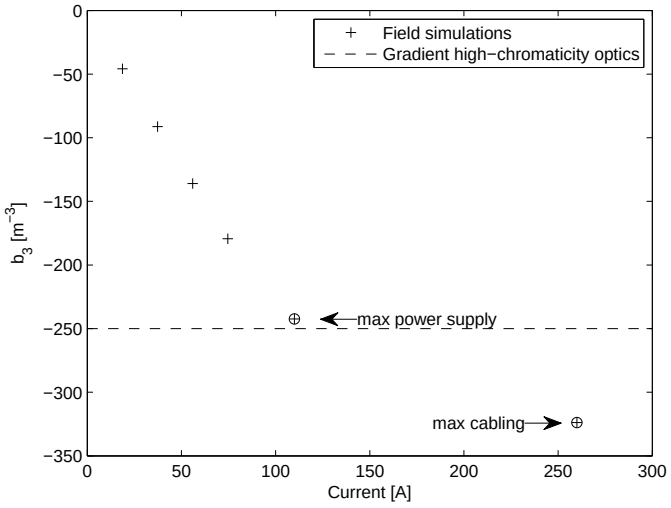

Figure 4.25: Simulated gradient strength as function of current for the SDend magnet. The maximum gradient that can be produced with the present power supply and cabling is marked, as well as the gradient strength needed for the high-chromaticity optics.

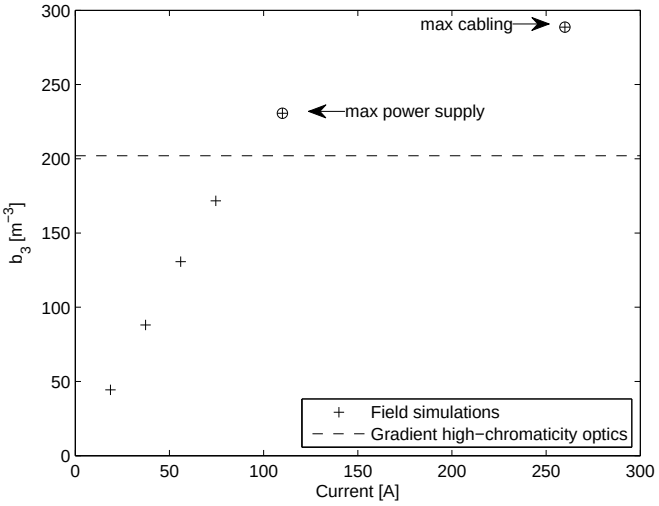

Figure 4.26: Simulated gradient strength as function of current for the SFm magnet. The maximum gradient that can be produced with the present power supply and cabling is marked, as well as the gradient strength needed for the high-chromaticity optics.

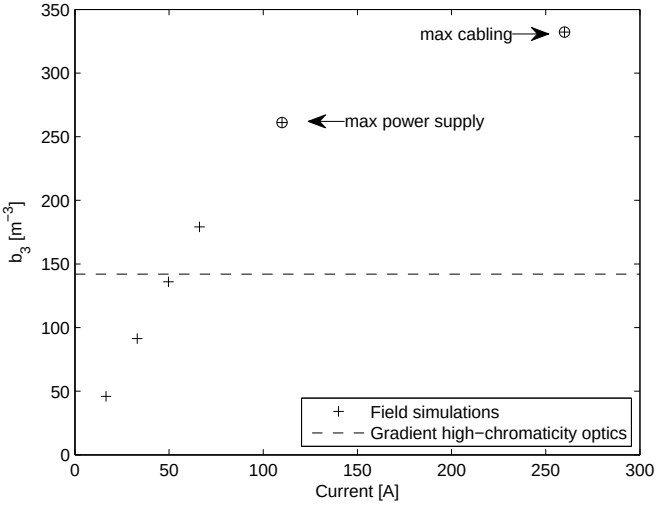

Figure 4.27: Simulated gradient strength as function of current for the SFo magnet. The maximum gradient that can be produced with the present power supply and cabling is marked, as well as the gradient strength needed for the high-chromaticity optics.

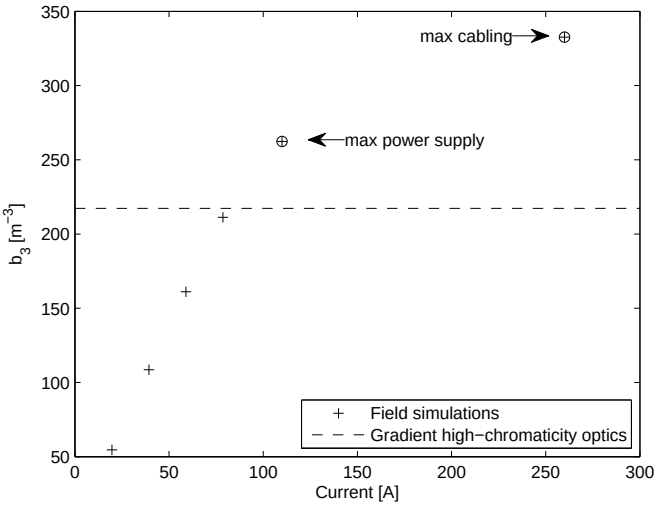

Figure 4.28: Simulated gradient strength as function of current for the SFi magnet. The maximum gradient that can be produced with the present power supply and cabling is marked, as well as the gradient strength needed for the high-chromaticity optics.

The gradient strengths for the octupole magnets from [30] with required strengths for the high-chromaticity optics are displayed in Fig. 4.29 - Fig. 4.31. Fig. 4.31 indicate that the gradient required for the high-chromaticity optics cannot be achieved for the OYY-magnet with present power supply, but the present cabling should be sufficient. For all other magnets the required gradient strengths for the high-chromaticity optics should be achievable to produce with the present power supplies.

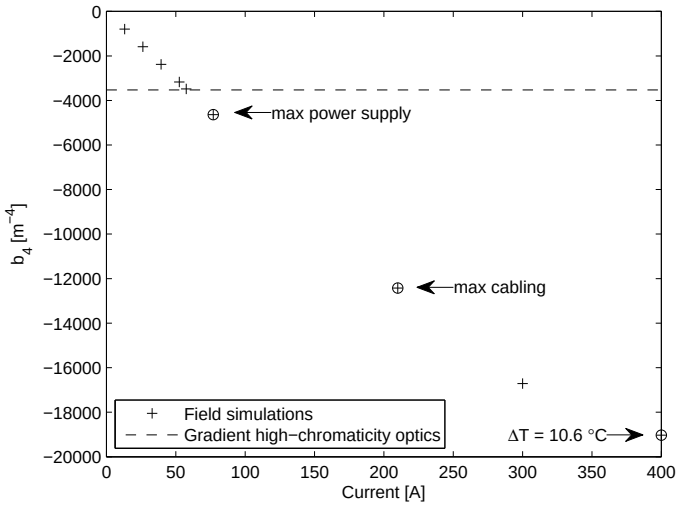

Figure 4.29: Simulated gradient strength as function of current for the OXX-magnet. The maximum gradient that can be produced with the present power supply and cabling is marked, as well as the gradient required for the high-chromaticity optics. The gradient simulations are taken from [30].

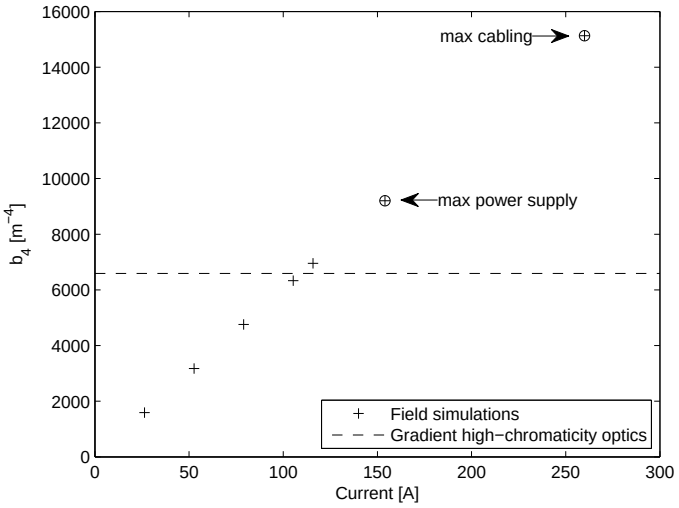

Figure 4.30: Simulated gradient strength as function of current for the OXY-magnet. The maximum gradient that can be produced with the present power supply and cabling is marked, as well as the gradient required for the high-chromaticity optics. The gradient simulations are taken from [30].

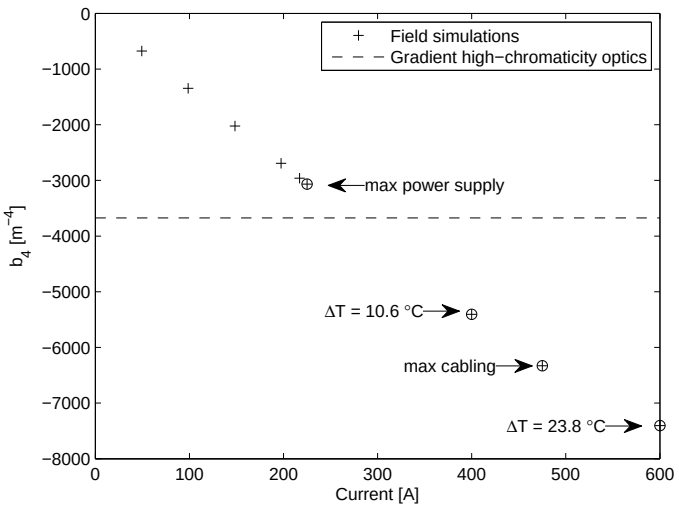

Figure 4.31: Simulated gradient strength as function of current for the OYY-magnet. The maximum gradient that can be produced with the present power supply and cabling is marked, as well as the gradient required for the high-chromaticity optics. The gradient simulations are taken from [30].

Chapter 5
Discussion and Conclusions

5.1 Performance of the High-chromaticity Optics

Both the chromatic tune shifts and the amplitude-dependent tune shifts are larger for the high-chromaticity optics than for the design optics. This results in a smaller dynamic aperture both on and off-momentum for the high-chromaticity optics, but the required aperture on and off-momentum are still fulfilled.

On-momentum frequency map analysis distinguishes two resonances. They are both of higher than 4th order and are not expected to be driven strongly since they originate from higher-order multipole content of the magnets. Comparison with the corresponding diffusion map shows that these resonance lines lie outside the required dynamic aperture and thus do not limit the possibility to fulfil this requirement. When errors are included the dynamic aperture is reduced, but the horizontal required aperture set by the injection process is still fulfilled. It is therefore expected that the reduction of on-momentum dynamic aperture could result in a reduced beam lifetime, but should not cause any serious problems for the injection process.

Off-momentum frequency map analysis shows several areas that might be problematic. Two 4th order resonances are recognised inside the desired momentum acceptance. Both are caused by normal octupole magnets and therefore can be driven. However, since they are 4th order resonances driven by weak octupoles they are not expected to cause severe problems. When errors are included the dynamic aperture is reduced as for the on-momentum case. For $\delta = \pm 4.5\%$ this is a serious issue since hardly any dynamic aperture remains. Especially for $\delta = -4.5\%$ the situation appears dramatic. However, the dynamic aperture with errors is non-zero for $\delta = \pm 4\%$ and $\delta = \pm 3.5\%$ indicating that a reduced lattice momentum acceptance might be achievable with the high-chromaticity optics. Although a momentum acceptance of $\pm 4.5\%$ cannot be ensured by the high-chromaticity optics, a momentum acceptance of roughly $\pm 3.5\%$ should be achievable since the resulting hor-

izontal dynamic aperture with errors are on the same scale as an aperture required for roughly ±3.5% momentum acceptance. When evaluating the results of the error studies the uncertainty of the error models and the poor statistics (only 20 seeds were used) should also be taken into consideration.

The Touschek lifetime can be considered the ultimate measure of performance of the optics since the dynamic aperture determines the momentum acceptance and the momentum acceptance in turn determines the Touschek lifetime. The Touschek lifetime of the high-chromaticity optics is calculated to be roughly 9 hours without errors whereas the corresponding Touschek lifetime for the design optics is roughly 14 hours. This is a considerable reduction of Touschek lifetime, but not unexpected because of the implications of the high-chromaticity optics on the dynamics. Since the purpose of the high-chromaticity optics is to be available as a short-term solution during commissioning should instability issues occur, the demand for a high Touschek lifetime is not as stringent as for the design optics. A Touschek lifetime that allows for machine studies to be performed is sufficient. The very rough estimate of Touschek lifetime reduction with errors indicates that the Touschek lifetime of the high-chromaticity optics will be sufficient, especially if the Landau cavities are tuned in, since the minimum local momentum acceptance with errors is expected to be between ±2% and ±3%. It is estimated that a momentum acceptance of roughly ±2% can be tolerated before the Touschek lifetime becomes too small for the high-chromaticity optics to be useful. However, this was just a very rough estimate and further studies need to be performed. The performed estimation reveals that the Touschek lifetime with errors present lies close to the minimum for a useful Touschek lifetime.

As previously stated, the dynamic aperture and the momentum acceptance determine the Touschek lifetime. The Touschek lifetime can be improved by enlarging the off-momentum dynamic aperture and it is therefore of interest to determine the limitations of the off-momentum dynamic aperture. It is apperent that the dynamic aperture is smaller for negative than for positive momentum deviations. From the off-momentum frequency map analysis it is found that a region with chaotic motion occurs around $\delta = -5\%$ and this is likely caused by the strong integer resonance $\nu_x = 42$. The chromatic tune footprint of the high-chromaticity optics extends over a large region and approaches $\nu_x = 42$ when reaching $\delta = -4.5\%$. Taking into consideration the amplitude-dependent tune shifts a plausible explanation is that the resonance $\nu_x = 42$ limits the dynamic aperture for negative momentum deviations. An effort to improve the dynamic aperture should therefore in a first stage focus on increasing the distance to the resonance $\nu_x = 42$.

5.2 Challenges for a High-chromaticity Optics

The correction of the linear chromaticity to +4 in both planes sets high demands on the nonlinear optics to achieve sufficiently large on and off-momentum dynamic aperture to ensure an efficient injection process and sufficient Touschek lifetime. Since the linear chromaticity is set to +4 there is a need for strong sextupole magnets and skillful optimisation of the chromatic tune footprint to accomplish small chromatic tune shifts which do not cross dangerous resonances. Due to the enlarged chromatic tune footprint caused by the increased linear chromaticity the demand for small amplitude-dependent tune shifts is further increased. A difficulty when optimising the amplitude-dependent tune shifts comes from the fact that $\partial\nu_x/\partial J_y = \partial\nu_y/\partial J_x$. This means that the optimisation always presents a compromise between these tune shifts. However, since the required vertical aperture is much smaller than the required horizontal aperture the focus can be put on minimising $\partial\nu_y/\partial J_x$ since $\partial\nu_x/\partial J_y$ will have less influence on the relevant amplitude-dependent tune footprint because of the small vertical apertures.

The strong sextupole magnets and the increased need for small amplitude-dependent tune shifts require strong octupole magnets. When the strength of the octupole magnets is considerably enlarged they start to have substantial effect on the chromatic tune shift via nonlinear dispersion. Then the chromatic tune shifts and the amplitude-dependent tune shifts have to be optimised with regard to each other. This means that the design approach to first tailor the chromatic tune shifts with the sextupole magnets and then the amplitude-dependent tune shifts with the octupole magnets needs to be interated to find possible candidates for high-chromaticity that then can be analysed and revised further. The possibility of finding a high-chromaticity optics with good performance is then not only a question of analysing what limits the performance, but also a question of design skill to produce a revised candidate with the properties that are desired according to the result of the analysis of previous candidates.

5.3 The Design Process

The process of finding good candidates for a high-chromaticity optics relies heavily upon the skills of the designer. Since a trial-and-error approach needs to be used it is a complex task to produce a candidate that fulfils all the desired requirements. The possibly of being successful is therefore improved with the number of iterations during which knowledge is gathered about how the tune shifts are affected by changes to the strength of the magnets and acquiring a feeling for what kind of design is possible to achieve. It is also of importance to have good knowledge of the tools that are used during the design process and to evaluate the performance of the design. Good knowledge of the tools makes it possible to use them in a more efficient manner and gather more information that is helpful when considering improvements to the design.

At the beginning of this work the design process focused on mimicking the chromatic tune shifts and amplitude-dependent tune shifts of the design optics. This was useful to find possible candidates for a high-chromaticity optics to further analyse and to learn about the tools used in the design process. However, later in the design process less effort was made on mimicking the design optics and instead the tune shifts were tailored according to estimations of what was possible to achieve based on gathered experience. During later iterations the result from analysis of the performance of earlier candidates is also available to determine which design options that would give improved performance of the high-chromaticity optics. Still, since the design process is based on a trial-and-error approach it is important to systemize the work to not get stuck in one's own way of thinking and instead possibly find new ways of making a design that has not been tested and analysed before. An idea for how this can be done is to not focus on trying to minimise the amplitude-dependent tune shifts but instead use them to improve poor situations created by the chromatic tune shifts. If the chromatic tune shifts comes close to a possibly dangerous resonance the amplitude-dependent tune shifts might be tailored so that the particles move away from the resonance instead of closer to it. Ideally, both small chromatic and amplitude-dependent tune shifts are desired but if small chromatic tune shifts cannot be achieved, due to for example a high linear chromaticity, small amplitude-dependent tune shifts might actually not be the optimal design.

5.4 Technical Limitations

The maximum field strengths that the magnets are able to produce set a restriction to the design process if the high-chromaticity optics should be able to operate in the real machine. According to the simulations of the maximum field strengths for the sextupole and octupole magnets they will be able to produce the necessary strength for the high-chromaticity optics with present cabling. For two of the magnets, SDend and OYY the present power supplies need to be replaced but for all other magnets the present power supplies are capable of producing the required gradients.

5.5 Conclusions

A high-chromaticity optics with linear chromaticity +4 in both planes has been developed for the MAX IV 3 GeV storage ring. The performance of the high-chromaticity optics is poorer than the performance of the design optics. The high-chromaticity optics has a smaller dynamic aperture than the design optics, especially for off-momentum particles. The momentum acceptance of the high-chromaticity optics is therefore expected to be lower than for the design optics. This results in a considerable reduction of the Touschek lifetime. The performance of the high-chromaticity optics is affected by increased chromatic tune shifts caused by the increased linear chromaticity interacting with increased amplitude-dependent tune shifts. The Touschek lifetime for the high-chromaticity optics under influence of imperfections require further studies, but a very rough estimate indicates Touschek lifetime will be sufficient to allow the optics to be applied in the MAX IV 3 GeV storage ring as a short term solution if instability issues should occur during commissioning. There also exist opportunities to redesign the high-chromaticity optics and perhaps further improve its performance.

Chapter 6
Further Work

Further iterations are suggested to improve the performance of the high-chromaticity optics. So far only a first iteration has been performed, but additional changes to the design and analysis of the resulting performance will increase the understanding of the limitations of the design and hopefully result in improvement. A more in-depth analysis of the Touschek lifetime is also necessary to get a more complete picture of the lifetime that can be achieved with the high-chromaticity optics. The influence from errors needs to be evaluated further since only a rough estimate was performed in the scope of this thesis. If a more profound analysis shows that the Touschek lifetime of the high-chromaticity optics is not sufficient it could become a necessity to improve the optics.

One possibility to be considered is a change of working point. By moving the working point one can attempt to move away from the integer resonance that currently limits the off-momentum dynamic aperture and possibly therefore enlarge the momentum acceptance.

The technical limitations proposed by the maximum strength of the magnets need further investigation since the studies performed in the scope of this thesis are just initial simulations. The cost for changing the required power supplies could also be evaluated to make a decision whether the high-chromaticity can be operated with present restrictions or if a high-chromaticity optics that uses only present power supplies needs to be developed.

In the scope of this work the effect of an optics with linear chromaticity $+4$ in both planes on the instabilities has not been evaluated. It has been assumed that operating the storage ring at a higher chromaticity would mitigate possible instability issues, but further investigation would be desirable before investing in new power supplies. The correction value $+4$ has been chosen somewhat arbitrarily and it is possible that instability issues could be resolved at a lower linear chromaticity. In such a case a high-chromaticity optics with better performance might be achievable since the constraints set

by the linear chromaticity are less stringent.

In this thesis, a trial-and-error approach has been used to find candidates for a high-chromaticity optics. A less traditonal approach that could be considered is to use multiobjective genetic algorithms (MOGA) to find better candidates. A MOGA optimisation starts by a random selection of possible solutions which then evolves into subsequent generations by mimicking natural selection processes. After a number of iterations this should result in a generation that represents the solutions that optimise all the different design objectives [34]. Using MOGA it could be possible to maximise the dynamic aperture while both constraining the linear chromaticities to +4 in both planes and setting a maximum limit to the magnet gradients [35]. This is especially interesting because of the complexity that arises when the strenghts of the octupoles are enlarged to the level when they start to affect the chromatic tune shifts. It then becomes difficult to find good candidates with the trial-and-error approach and MOGA could prove more useful.

References

[1] Wille, K., 2000, *The Physics of Particle Accelerators*, Oxford University Press.

[2] MAX IV Laboratory, 2010, *Detailed Design Report MAX IV Facility*, MAX IV Laboratory.

[3] Wilson, E., 2001, *An Introduction to Particle Accelerators*, Oxford University Press.

[4] Eriksson, M., Ahlbäck, J., Andersson, Å., Johansson, M., Kumbaro, D., Leemann, S.C., Lenngren, C., Lilja, P., Lindau, F., Lindgren, L.-J., Malmgren, L., Modeér, J., Nilsson, R., Sjöström, M., Tagger, J., Tavares, P. F., Thorin, S., Wallén, E., Werin, S., 2011, *The MAX IV Synchrotron Light Source*, Proceedings of the 2011 International Particle Accelerator Conference, September 4-9, San Sebastián, Spain, pp. 3026-3028.

[5] MAX IV Laboratory, *Research*, https://www.maxlab.lu.se/research, available 2013-09-15.

[6] Leemann, S.C., Andersson, Å., Eriksson, M., Lindgren, L-.J., and Wallén, E., 2009, *Beam Dynamics and Expected Performance of Sweden's New Storage-ring Light Source: MAX IV*, Physcial Review Special Topics - Accelerators and Beams, Vol. 12, No. 12, 120701.

[7] Wiedemann, H., 2007, *Particle Accelerator Physics*, Springer.

[8] Leemann, S.C., 2012 (Updated 2013), *Updates to the MAX IV 3 GeV Storage Ring Lattice, MAX-lab Internal Note 20121107*, MAX IV Laboratory.

[9] Georgsson, M., 2001, *Landau Cavities in Third Generation Synchrotron Light Sources*, Proceedings of the 2001 Particle Accelerator Conference, June 18-22, Chicago, USA, pp. 2689-2691.

[10] Chang, L.H, Wang, Ch., Lau, W.K., and Kuo, C.C., 1997, *Effects of the Landau Cavity on the Electron Beam*, Proceedings of the 1997 Particle Accelerator Conference, May 12-16, Vancouver, USA, pp. 1691-1693.

[11] Griffiths, J., 2008, *Introduction to Electrodynamics*, Pearson Benjamin Cummings.

[12] Rossbach, J. and Schmüser, P., 1993, *Basic Course on Accelerator Physics*. Proceedings of CERN Accelerator School: 5th General Accelerator Physics Course, September 7-18, Jyväskylä, Finland, pp. 27.

[13] Roblin, Y., 2008, *Normal and skew multipole terms in the dipoles and quadrupoles of the 12 GeV CEBAF upgrade.*JLab Tech Notes JLAB-TN-08-042, Jefferson Laboratory.

[14] Plasma & Beam Physics Research Facility, Chiang Mai University, Deparment of Physics & Materials Science, Faculty of Science, *Accelerator Magnet Theory*, http://www.fnrf.science.cmu.ac.th/magnets.html, available 2013-09-05.

[15] Bergstrom, J. C., 2006, *Jack's Book (On Beam Instabilities and Other Things)*, Canadian Light Source.

[16] Klein, M., Skripka, G., Tavares, P. F., Wallén, E., 2013, *Study of Collective Beam Instabilities for the MAX IV 3 GeV Ring*, Proceedings of IPAC2013, May 12-14, Shanghai, China, pp, 1730-1732.

[17] Smaluk, V. V., 2009, *Mechanisms for Suppressing the Transverse Mode Coupling Instability in a Circular Accelerator*, Journal of Experimental and Theoretical Physics, Vol. 108, No. 3, pp. 482-489.

[18] Tavares, P. F., Nagaoka, and R., Günzel, T. F., 2011, *Collective Effects in the MAX IV 3 GeV Ring*, Proceedings of International Accelerator Conference 2011, September 4-9, San Sebastián, Spain, pp.754-756.

[19] Streun, A., *Non-linearities in Light Sources*, Proceedings of CERN Accelerator School: Intermediate Course on Accelerator Physics, September 15-16, Zeuthen, pp.203-216.

[20] Leemann, S. C., and Streun, A., 2011, *Perspectives for future light source lattices incorporating yet uncommon magnets*, Physical Review Special Topics - Accelerators and Beams, Vol. 14., No 3., 030701.

[21] Leemann, S. C., 2011, *MAX IV 3 GeV Storage Ring - Dynamic Aperture & Injection Revisited*, 3rd MAX MAC Meeting.

[22] Sayed, H. K, Krafft, G., and Bogacz, A., 2011, *Touschek Scattering*, US Particle Accelerator School Lecture Notes, Lecture 18 Touschek lifetime, Jefferson Laboratory.

[23] Streun, A., 1997 (Corr. 2008), *Momentum acceptance and Touschek lifetime*, SLS Note 18/97, Paul Scherrer Institut.

[24] Boccheta, C. J., 2003, *Intra Beam Scattering*, Proceedings of CERN Accelerator School: Synchrotron Radiation and Free Electron Lasers, July 2-9, Brunnen, Switzerland.

[25] Leemann, S. C., private communication 2013.

[26] Streun, A., 2012, *OPA version 3.39*, http://people.web.psi.ch/streun/opa/, available 2013-09-05.

[27] Bengtsson, J., *Tracy-2 User's Manual*, unpublished.

[28] Boccheta, C. J., 2003, *Frequency Map Analysis - A method to study the stability of a dynamical system*, Proceedings of CERN Accelerator School: Synchrotron Radiation and Free Electron Lasers, July 2-9, Brunnen, Switzerland.

[29] Johansson, M., *3 GeV ring magnets 2D & 3D simulations, MJ130614*, private communciation 2013.

[30] Johansson, M., *8poles max strength, MJ130617*, private communication 2013.

[31] Tavares, P. F., *MAXIVMagnetPowerSupplies*, Excel document, private communication 2013.

[32] Elproman - specialkabelhuset, *Strömbelastning för isolerade starkströmsledningar med kopparledare.* https://www.elproman.se/Welcome/Default.aspx?scenarioID=1070, available 2013-09-15.

[33] Johansson, M., *Magnet list, MAX IV 3GeV storage ring, MJ120326*, Excel document, private communication 2013.

[34] Yang, L., Robin, D., Sannibale, F., Steier, C., Wan, W., *Global optimization of an accelerator lattice using multiobjective genetic algorithms*, 2009, Nuclear Instuments and Methods in Physics Research, Vol. 609, pp. 50-57.

[35] Yang, L., Yongjun, L., Gao, W., Krinsky, S. *Multiobjective optimization of dynamic aperture*, 2011, Physical Review Special Topics - Accelerators and Beams, Vol. 14, 054001.